DESY-05-050
Mar 2005

An NLO QCD analysis of inclusive cross-section and jet-production data from the ZEUS experiment

ZEUS Collaboration

Abstract

The ZEUS inclusive differential cross-section data from HERA, for charged and neutral current processes taken with e^+ and e^- beams, together with differential cross-section data on inclusive jet production in e^+p scattering and dijet production in γp scattering, have been used in a new NLO QCD analysis to extract the parton distribution functions of the proton. The input of jet-production data constrains the gluon and allows an accurate extraction of $\alpha_s(M_Z)$ at NLO;

$$\alpha_s(M_Z) = 0.1183 \pm 0.0028(\text{exp.}) \pm 0.0008(\text{model}).$$

An additional uncertainty from the choice of scales is estimated as ± 0.005. This is the first extraction of $\alpha_s(M_Z)$ from HERA data alone.

The ZEUS Collaboration

S. Chekanov, M. Derrick, S. Magill, S. Miglioranzi[1], B. Musgrave, J. Repond, R. Yoshida
Argonne National Laboratory, Argonne, Illinois 60439-4815, USA [n]

M.C.K. Mattingly
Andrews University, Berrien Springs, Michigan 49104-0380, USA

N. Pavel, A.G. Yagües Molina
Institut für Physik der Humboldt-Universität zu Berlin, Berlin, Germany

P. Antonioli, G. Bari, M. Basile, L. Bellagamba, D. Boscherini, A. Bruni, G. Bruni, G. Cara Romeo, L. Cifarelli, F. Cindolo, A. Contin, M. Corradi, S. De Pasquale, P. Giusti, G. Iacobucci, A. Margotti, A. Montanari, R. Nania, F. Palmonari, A. Pesci, A. Polini, L. Rinaldi, G. Sartorelli, A. Zichichi
University and INFN Bologna, Bologna, Italy [e]

G. Aghuzumtsyan, D. Bartsch, I. Brock, S. Goers, H. Hartmann, E. Hilger, P. Irrgang, H.-P. Jakob, O.M. Kind, U. Meyer, E. Paul[2], J. Rautenberg, R. Renner, K.C. Voss[3], M. Wang, M. Wlasenko
Physikalisches Institut der Universität Bonn, Bonn, Germany [b]

D.S. Bailey[4], N.H. Brook, J.E. Cole, G.P. Heath, T. Namsoo, S. Robins
H.H. Wills Physics Laboratory, University of Bristol, Bristol, United Kingdom [m]

M. Capua, S. Fazio, A. Mastroberardino, M. Schioppa, G. Susinno, E. Tassi
Calabria University, Physics Department and INFN, Cosenza, Italy [e]

J.Y. Kim, K.J. Ma[5]
Chonnam National University, Kwangju, South Korea [g]

M. Helbich, Y. Ning, Z. Ren, W.B. Schmidke, F. Sciulli
Nevis Laboratories, Columbia University, Irvington on Hudson, New York 10027 [o]

J. Chwastowski, A. Eskreys, J. Figiel, A. Galas, K. Olkiewicz, P. Stopa, D. Szuba, L. Zawiejski
Institute of Nuclear Physics, Cracow, Poland [i]

L. Adamczyk, T. Bołd, I. Grabowska-Bołd, D. Kisielewska, A.M. Kowal, J. Łukasik, M. Przybycień, L. Suszycki, J. Szuba[6]
Faculty of Physics and Applied Computer Science, AGH-University of Science and Technology, Cracow, Poland [p]

A. Kotański[7], W. Słomiński
Department of Physics, Jagellonian University, Cracow, Poland

V. Adler, U. Behrens, I. Bloch, K. Borras, G. Drews, J. Fourletova, A. Geiser, D. Gladkov, P. Göttlicher[8], O. Gutsche, T. Haas, W. Hain, C. Horn, B. Kahle, U. Kötz, H. Kowalski, G. Kramberger, D. Lelas[9], H. Lim, B. Löhr, R. Mankel, I.-A. Melzer-Pellmann, C.N. Nguyen, D. Notz, A.E. Nuncio-Quiroz, A. Raval, R. Santamarta, U. Schneekloth, H. Stadie, U. Stösslein, G. Wolf, C. Youngman, W. Zeuner
Deutsches Elektronen-Synchrotron DESY, Hamburg, Germany

S. Schlenstedt
Deutsches Elektronen-Synchrotron DESY, Zeuthen, Germany

G. Barbagli, E. Gallo, C. Genta, P. G. Pelfer
University and INFN, Florence, Italy [e]

A. Bamberger, A. Benen, F. Karstens, D. Dobur, N.N. Vlasov[10]
Fakultät für Physik der Universität Freiburg i.Br., Freiburg i.Br., Germany [b]

P.J. Bussey, A.T. Doyle, W. Dunne, J. Ferrando, J. Hamilton, D.H. Saxon, I.O. Skillicorn
Department of Physics and Astronomy, University of Glasgow, Glasgow, United Kingdom [m]

I. Gialas[11]
Department of Engineering in Management and Finance, Univ. of Aegean, Greece

T. Carli[12], T. Gosau, U. Holm, N. Krumnack[13], E. Lohrmann, M. Milite, H. Salehi, P. Schleper, T. Schörner-Sadenius, S. Stonjek[14], K. Wichmann, K. Wick, A. Ziegler, Ar. Ziegler
Hamburg University, Institute of Exp. Physics, Hamburg, Germany [b]

C. Collins-Tooth[15], C. Foudas, C. Fry, R. Gonçalo[16], K.R. Long, A.D. Tapper
Imperial College London, High Energy Nuclear Physics Group, London, United Kingdom [m]

M. Kataoka[17], K. Nagano, K. Tokushuku[18], S. Yamada, Y. Yamazaki
Institute of Particle and Nuclear Studies, KEK, Tsukuba, Japan [f]

A.N. Barakbaev, E.G. Boos, N.S. Pokrovskiy, B.O. Zhautykov
Institute of Physics and Technology of Ministry of Education and Science of Kazakhstan, Almaty, Kazakhstan

D. Son
Kyungpook National University, Center for High Energy Physics, Daegu, South Korea [g]

J. de Favereau, K. Piotrzkowski
Institut de Physique Nucléaire, Université Catholique de Louvain, Louvain-la-Neuve, Belgium [q]

F. Barreiro, C. Glasman[19], M. Jimenez, L. Labarga, J. del Peso, J. Terrón, M. Zambrana
Departamento de Física Teórica, Universidad Autónoma de Madrid, Madrid, Spain [l]

F. Corriveau, C. Liu, M. Plamondon, A. Robichaud-Veronneau, R. Walsh, C. Zhou
Department of Physics, McGill University, Montréal, Québec, Canada H3A 2T8 [a]

T. Tsurugai
Meiji Gakuin University, Faculty of General Education, Yokohama, Japan [f]

A. Antonov, B.A. Dolgoshein, I. Rubinsky, V. Sosnovtsev, A. Stifutkin, S. Suchkov
Moscow Engineering Physics Institute, Moscow, Russia [j]

R.K. Dementiev, P.F. Ermolov, L.K. Gladilin, I.I. Katkov, L.A. Khein, I.A. Korzhavina, V.A. Kuzmin, B.B. Levchenko, O.Yu. Lukina, A.S. Proskuryakov, L.M. Shcheglova, D.S. Zotkin, S.A. Zotkin
Moscow State University, Institute of Nuclear Physics, Moscow, Russia [k]

I. Abt, C. Büttner, A. Caldwell, X. Liu, J. Sutiak
Max-Planck-Institut für Physik, München, Germany

N. Coppola, G. Grigorescu, A. Keramidas, E. Koffeman, P. Kooijman, E. Maddox, H. Tiecke, M. Vázquez, L. Wiggers
NIKHEF and University of Amsterdam, Amsterdam, Netherlands [h]

N. Brümmer, B. Bylsma, L.S. Durkin, T.Y. Ling
Physics Department, Ohio State University, Columbus, Ohio 43210 [n]

P.D. Allfrey, M.A. Bell, A.M. Cooper-Sarkar, A. Cottrell, R.C.E. Devenish, B. Foster, C. Gwenlan[20], T. Kohno, K. Korcsak-Gorzo, S. Patel, P.B. Straub, R. Walczak
Department of Physics, University of Oxford, Oxford United Kingdom [m]

P. Bellan, A. Bertolin, R. Brugnera, R. Carlin, R. Ciesielski, F. Dal Corso, S. Dusini, A. Garfagnini, S. Limentani, A. Longhin, L. Stanco, M. Turcato
Dipartimento di Fisica dell' Università and INFN, Padova, Italy [e]

E.A. Heaphy, F. Metlica, B.Y. Oh, J.J. Whitmore[21]
Department of Physics, Pennsylvania State University, University Park, Pennsylvania 16802 [o]

Y. Iga
Polytechnic University, Sagamihara, Japan [f]

G. D'Agostini, G. Marini, A. Nigro
Dipartimento di Fisica, Università 'La Sapienza' and INFN, Rome, Italy [e]

J.C. Hart
Rutherford Appleton Laboratory, Chilton, Didcot, Oxon, United Kingdom [m]

H. Abramowicz[22], A. Gabareen, S. Kananov, A. Kreisel, A. Levy
Raymond and Beverly Sackler Faculty of Exact Sciences, School of Physics, Tel-Aviv University, Tel-Aviv, Israel [d]

M. Kuze
Department of Physics, Tokyo Institute of Technology, Tokyo, Japan [f]

S. Kagawa, T. Tawara
Department of Physics, University of Tokyo, Tokyo, Japan [f]

R. Hamatsu, H. Kaji, S. Kitamura[23], K. Matsuzawa, O. Ota, Y.D. Ri
Tokyo Metropolitan University, Department of Physics, Tokyo, Japan [f]

M. Costa, M.I. Ferrero, V. Monaco, R. Sacchi, A. Solano
Università di Torino and INFN, Torino, Italy [e]

M. Arneodo, M. Ruspa
Università del Piemonte Orientale, Novara, and INFN, Torino, Italy [e]

S. Fourletov, J.F. Martin
Department of Physics, University of Toronto, Toronto, Ontario, Canada M5S 1A7 [a]

J.M. Butterworth[24], R. Hall-Wilton, T.W. Jones, J.H. Loizides[25], M.R. Sutton[4], C. Targett-Adams, M. Wing
Physics and Astronomy Department, University College London, London, United Kingdom [m]

J. Ciborowski[26], G. Grzelak, P. Kulinski, P. Łużniak[27], J. Malka[27], R.J. Nowak, J.M. Pawlak, J. Sztuk[28], T. Tymieniecka, A. Tyszkiewicz[27], A. Ukleja, J. Ukleja[29], A.F. Żarnecki
Warsaw University, Institute of Experimental Physics, Warsaw, Poland

M. Adamus, P. Plucinski
Institute for Nuclear Studies, Warsaw, Poland

Y. Eisenberg, D. Hochman, U. Karshon, M.S. Lightwood
Department of Particle Physics, Weizmann Institute, Rehovot, Israel [c]

E. Brownson, T. Danielson, A. Everett, D. Kçira, S. Lammers, L. Li, D.D. Reeder, M. Rosin, P. Ryan, A.A. Savin, W.H. Smith
Department of Physics, University of Wisconsin, Madison, Wisconsin 53706, USA [n]

S. Dhawan
Department of Physics, Yale University, New Haven, Connecticut 06520-8121, USA [n]

S. Bhadra, C.D. Catterall, Y. Cui, G. Hartner, S. Menary, U. Noor, M. Soares, J. Standage, J. Whyte
Department of Physics, York University, Ontario, Canada M3J 1P3 [a]

[1] also affiliated with University College London, UK
[2] retired
[3] now at the University of Victoria, British Columbia, Canada
[4] PPARC Advanced fellow
[5] supported by a scholarship of the World Laboratory Björn Wiik Research Project
[6] partly supported by Polish Ministry of Scientific Research and Information Technology, grant no.2P03B 12625
[7] supported by the Polish State Committee for Scientific Research, grant no. 2 P03B 09322
[8] now at DESY group FEB, Hamburg, Germany
[9] now at LAL, Université de Paris-Sud, IN2P3-CNRS, Orsay, France
[10] partly supported by Moscow State University, Russia
[11] also affiliated with DESY
[12] now at CERN, Geneva, Switzerland
[13] now at Baylor University, USA
[14] now at University of Oxford, UK
[15] now at the Department of Physics and Astronomy, University of Glasgow, UK
[16] now at Royal Holloway University of London, UK
[17] also at Nara Women's University, Nara, Japan
[18] also at University of Tokyo, Japan
[19] Ramón y Cajal Fellow
[20] PPARC Postdoctoral Research Fellow
[21] on leave of absence at The National Science Foundation, Arlington, VA, USA
[22] also at Max Planck Institute, Munich, Germany, Alexander von Humboldt Research Award
[23] present address: Tokyo Metropolitan University of Health Sciences, Tokyo 116-8551, Japan
[24] also at University of Hamburg, Germany, Alexander von Humboldt Fellow
[25] partially funded by DESY
[26] also at Łódź University, Poland
[27] Łódź University, Poland
[28] Łódź University, Poland, supported by the KBN grant 2P03B12925
[29] supported by the KBN grant 2P03B12725

[a] supported by the Natural Sciences and Engineering Research Council of Canada (NSERC)

[b] supported by the German Federal Ministry for Education and Research (BMBF), under contract numbers HZ1GUA 2, HZ1GUB 0, HZ1PDA 5, HZ1VFA 5

[c] supported in part by the MINERVA Gesellschaft für Forschung GmbH, the Israel Science Foundation (grant no. 293/02-11.2), the U.S.-Israel Binational Science Foundation and the Benozyio Center for High Energy Physics

[d] supported by the German-Israeli Foundation and the Israel Science Foundation

[e] supported by the Italian National Institute for Nuclear Physics (INFN)

[f] supported by the Japanese Ministry of Education, Culture, Sports, Science and Technology (MEXT) and its grants for Scientific Research

[g] supported by the Korean Ministry of Education and Korea Science and Engineering Foundation

[h] supported by the Netherlands Foundation for Research on Matter (FOM)

[i] supported by the Polish State Committee for Scientific Research, grant no. 620/E-77/SPB/DESY/P-03/DZ 117/2003-2005 and grant no. 1P03B07427/2004-2006

[j] partially supported by the German Federal Ministry for Education and Research (BMBF)

[k] supported by RF Presidential grant N 1685.2003.2 for the leading scientific schools and by the Russian Ministry of Education and Science through its grant for Scientific Research on High Energy Physics

[l] supported by the Spanish Ministry of Education and Science through funds provided by CICYT

[m] supported by the Particle Physics and Astronomy Research Council, UK

[n] supported by the US Department of Energy

[o] supported by the US National Science Foundation

[p] supported by the Polish Ministry of Scientific Research and Information Technology, grant no. 112/E-356/SPUB/DESY/P-03/DZ 116/2003-2005 and 1 P03B 065 27

[q] supported by FNRS and its associated funds (IISN and FRIA) and by an Inter-University Attraction Poles Programme subsidised by the Belgian Federal Science Policy Office

1 Introduction

Since the advent of HERA, considerable progress has been made in the determination of the parton distribution functions (PDFs) of the proton. Precise knowledge of the PDFs, and of the strong coupling constant, $\alpha_s(M_Z)$, is crucial for an understanding of proton structure. Moreover, it is required for any calculation of cross sections at hadron colliders both for Standard Model physics and for the discovery of physics beyond the Standard Model.

The PDFs are usually determined in global fits [1–3] made within the conventional DGLAP formalism [4–7] at next-to-leading order (NLO). Such fits use data from many different experiments, with the inclusive cross-section data from deep inelastic scattering (DIS) experiments providing the major source of information. The wide kinematic range covered by the HERA DIS data [8–10], as well as their precision, has allowed the determination of PDFs across a broad range of phase space spanned by the fractional proton momentum carried by the struck quark, Bjorken x, and the negative squared four-momentum transfer between the lepton and nucleon, Q^2. The high-statistics HERA neutral current e^+p data determine the low-x sea and gluon distributions, whereas the fixed-target data, taken at lower centre-of-mass energy, determine the valence distributions and the higher-x sea distributions.

The gluon PDF contributes only indirectly to the inclusive DIS cross sections. However it makes a direct contribution to jet cross sections through boson-gluon and quark-gluon scattering. Tevatron high-E_T jet data [11,12] have been used to constrain the gluon in the fits of MRST [1,2] and CTEQ [3]. However, these data suffer from very large correlated systematic uncertainties from a variety of sources. For example, the total systematic uncertainty of CDF data is $\sim 60\%$ over its full E_T range. In the present paper, ZEUS neutral current e^+p DIS inclusive jet cross sections [13] and direct photoproduction dijet cross sections [14] have been used to constrain the gluon. These cross sections have only $\sim 5\%$ total systematic uncertainty, mainly due to the absolute energy-scale uncertainty of the jets.

These jet data were used, together with ZEUS data on neutral and charged current (NC and CC) e^+p and e^-p DIS inclusive cross sections [15–20], as inputs to an NLO QCD DGLAP analysis in order to determine the PDFs. This fit is called the ZEUS-JETS fit.

In the ZEUS-JETS fit, the lower Q^2 NC inclusive cross-section data determine the low-x sea and gluon distributions[1] and the high Q^2 NC and CC inclusive cross sections determine the valence distributions. The use of ZEUS data alone eliminates the uncertainty from heavy-target corrections required in global analyses in which the νFe and μD fixed-target

[1] The HERA kinematics is such that the lower-Q^2 data are also at low x.

data, together with isospin-symmetry constraints between u and d in the proton and neutron, have been used for determining the valence distributions. The jet cross-section data constrain the mid- to high-x ($x \approx 0.01 - 0.5$) gluon PDF. The predictions for the jet cross sections are calculated to NLO in QCD and are used in the fit rigorously, rather than approximately as in previous fits [1–3]. The quality of the fit establishes that NLO QCD is able simultaneously to describe both inclusive cross sections and jet cross sections, thereby providing a compelling demonstration of QCD factorisation.

The value of $\alpha_s(M_Z)$ is fixed in most PDF fits; for the ZEUS-JETS fit, the value $\alpha_s(M_Z) = 0.118$ [21] is used. A simultaneous fit for $\alpha_s(M_Z)$ and the PDF parameters, called the ZEUS-JETS-α_s fit, has also been made. This fit accounts for the correlation between $\alpha_s(M_Z)$ and the gluon shape. The addition of the jet production data provides enough constraints to give an accurate determination of $\alpha_s(M_Z)$ despite this correlation.

The PDFs are presented with full accounting for uncertainties from correlated systematic errors. Performing an analysis within a single experiment has considerable advantages in this respect since global fits have found significant tensions between different data sets [1]. In the present analysis, the contribution to the PDF uncertainties from correlated experimental uncertainties and normalisation uncertainties is significantly reduced in comparison to the previous ZEUS-S global fit analysis [8], which used data from many different DIS experiments.

This paper is organised as follows. In Section 2, the theoretical background is reviewed briefly and in Section 3, the method of analysis is outlined, with particular emphasis on the new features needed to include the jet cross sections in the fit. In Section 4, the ZEUS-JETS fit is compared to data and the extracted parton distributions and their experimental uncertaintes are presented. Model uncertainties are discussed and a comparison is made to the Tevatron jet data. In Section 5, the analysis is extended to the evaluation of $\alpha_s(M_Z)$ in the ZEUS-JETS-α_s fit and the uncertainties on $\alpha_s(M_Z)$ from theoretical sources are discussed. Section 6 gives a summary and conclusions.

2 Theoretical Background

The kinematics of deep inelastic lepton-nucleon scattering are described in terms of the variables Q^2, Bjorken x and y, the fractional energy transfer between the lepton and hadron systems. The differential cross sections for the NC DIS process are given in terms of structure functions by

$$\frac{d^2\sigma^{\rm NC}(e^{\pm}p)}{dxdQ^2} = \frac{2\pi\alpha^2}{xQ^4}\left[Y_+\,F_2(x,Q^2) - y^2\,F_L(x,Q^2) \mp Y_-\,xF_3(x,Q^2)\right],$$

where $Y_\pm = 1 \pm (1-y)^2$. The structure functions F_2 and xF_3 are directly related to quark distributions, and their Q^2 dependence, or scaling violation, is predicted by perturbative QCD. At $Q^2 \lesssim 1000$ GeV^2, the charged lepton-hadron cross section is dominated by photon exchange and the structure function F_2. For $x \lesssim 10^{-2}$, F_2 is sea-quark dominated and its Q^2 dependence is driven by the gluon contribution, such that HERA data provide crucial information on both quark and gluon distributions. The longitudinal structure function F_L is only important at high y and is calculated, in perturbative QCD, from the quark and gluon distributions [22]. At high Q^2, the structure function xF_3 becomes increasingly important; it provides information on valence quark distributions. The CC interactions are sensitive to the flavour of the valence distributions at high x since their (LO) cross sections are given by

$$\frac{d^2\sigma^{\rm CC}(e^+p)}{dxdQ^2} = \frac{G_F^2 M_W^4}{2\pi x(Q^2+M_W^2)^2} x\left[(\bar{u}+\bar{c}) + (1-y)^2(d+s)\right],$$

$$\frac{d^2\sigma^{\rm CC}(e^-p)}{dxdQ^2} = \frac{G_F^2 M_W^4}{2\pi x(Q^2+M_W^2)^2} x\left[(u+c) + (1-y)^2(\bar{d}+\bar{s})\right],$$

where the parton distributions u, d, s, c are functions of x and Q^2. Thus the e^-p CC cross section gives information on the u valence quark at high x, whereas the e^+p CC cross section gives information on the d valence quark at high x. This is particularly important since this process is a direct probe of the d valence quark on a proton target at high Q^2. Determinations of the d valence distribution have previously been dominated by low Q^2 data using isoscalar iron or deuterium targets. Such determinations are subject to uncertainties from higher-twist contributions, heavy-target and binding corrections and isospin-symmetry assumptions.

The inclusive cross-section data depend directly on the quark distributions, but the gluon distribution affects these cross sections indirectly through the scaling violations. Perturbative QCD predicts the rate at which the quark distributions evolve with the scale Q through the DGLAP equation

$$\frac{dq_i(x,Q^2)}{d\ln Q^2} = \frac{\alpha_s(Q^2)}{2\pi}\int_x^1 \frac{dy}{y}\left[\sum_j q_j(y,Q^2)P_{q_iq_j}\left(\frac{x}{y}\right) + g(y,Q^2)P_{q_ig}\left(\frac{x}{y}\right)\right], \qquad (1)$$

where the 'splitting function' $P_{ij}(z)$ represents the probability of a parton (either quark or gluon) j emitting a quark i with momentum fraction z of that of the parent parton. Thus the gluon distribution can be obtained indirectly from the scaling violations of the quark distributions. The parameters that describe the gluon shape and the value of the strong coupling constant, $\alpha_s(M_Z)$, are correlated through the DGLAP equations.

The QCD processes that give rise to scaling violations in the inclusive cross sections, namely the QCD-Compton (QCDC) and boson-gluon-fusion (BGF) processes, are observed as events with distinct jets in the final state provided that the energy and momentum transfer are large enough. The cross section for QCDC scattering depends on $\alpha_s(M_Z)$ and the quark PDFs. For HERA kinematics, this process dominates the jet cross section at large scales, where the quark densities are well known from the inclusive cross-section data, so that the value of $\alpha_s(M_Z)$ may be extracted without strong correlation to the shape of the gluon PDF. The cross section for the BGF process depends on $\alpha_s(M_Z)$ and the gluon PDF so that measurements of jet cross sections also provide a direct determination of the gluon density.

3 Analysis Method

The present analysis was performed within the Standard Model conventional paradigm of leading-twist NLO QCD. The QCD predictions for the PDFs were obtained by solving the DGLAP evolution equations at NLO. These equations yield the PDFs at all values of Q^2 provided they are parameterised as functions of x at some input scale Q_0. The programme QCDNUM [23] was used to perform the evolution.

The applicability of the leading-twist, NLO DGLAP formalism to HERA data was investigated in the previous ZEUS analysis [8], and suitable data cuts were defined. All the present data lie above these cuts. The data sets fitted in this analysis and their kinematic coverage are presented in Table 1. In total there are 577 data points from a total luminosity of 112 pb^{-1} from the HERA-I (1992-2000) running period.

Full account has been taken of correlated experimental systematic uncertainties using the Offset method, described in the previous ZEUS-S PDF analysis [8][2]. There are 22 independent sources of correlated systematic uncertainty and 4 independent normalisations for the data sets in the present analysis. The number of correlated systematic uncertainties for each data set, their normalisations and the correlations between the data sets are detailed in Table 1.

3.1 Inclusive cross-section data

The inclusive cross-section data used in the fits were reduced double differential cross-sections in x and Q^2 from: NC e^+p scattering [15, 19]; NC e^-p scattering [17]; CC e^+p scattering [16, 20]; and CC e^-p scattering [18].

[2] Different treatments of experimental uncertainties in PDF analyses are discussed extensively elsewhere [24–26]. The Offset method gives conservative PDF uncertainty estimates.

The NLO QCD predictions for the structure functions, which enter into the expressions for the cross sections, were obtained by convoluting the PDFs with the QCD coefficient functions appropriate to the process. It is necessary to specify the scheme and scale choice for the calculations. The renormalisation and factorisation scales for the inclusive DIS processes were chosen to be Q. The DGLAP equations were solved in the $\overline{\mathrm{MS}}$ scheme. For heavy-quark production, the general-mass variable flavour-number scheme of Thorne and Roberts (TRVFN) [27] was used in order to interpolate correctly between threshold behaviour and high-scale behaviour for heavy quarks, as discussed in the ZEUS-S analysis [8]. The values of the heavy quark masses used were $m_c = 1.35$ GeV and $m_b = 4.3$ GeV. Variation of these values in the ranges $1.2 < m_c < 1.5$ GeV and $4.0 < m_b < 4.6$ GeV produced changes in the PDF parameters that are negligible in comparison to the experimental uncertainties.

3.2 Jet data

The jet data used in the fits were: DIS inclusive jet differential cross sections as a function of the transverse energy in the Breit frame, E_T^B, for different Q^2 bins [13]; photoproduction dijet cross sections as a function of the transverse energy of the most energetic jet, E_T^{jet1}, in the laboratory frame, for different jet-pseudorapidity ranges [14]. The systematic uncertainty from the absolute jet energy scale was fully correlated between these two sets of data.

The cross-section predictions for photoproduced jets are sensitive to the choice of the input photon PDFs. The AFG photon PDF [28] has been used in the fits. In order to minimise sensitivity to this choice, the analysis has been restricted to use only the 'direct' photoproduction cross sections. These are defined by the cut $x_\gamma^{\mathrm{obs}} > 0.75$, where x_γ^{obs} is a measure of the fraction of the photon's momentum that enters into the hard scatter [14, 29, 30].

The programme of Frixione and Ridolfi [31] was used to compute NLO QCD cross sections for photoproduced dijets and Disent [32] was used to compute NLO QCD cross sections for jet production in DIS. These programmes treat the heavy quarks in a massless scheme. However all the jet data are at scales sufficiently high that the TRVFN scheme and the zero-mass variable flavour number scheme (ZMVFN) are equivalent. The calculation of the NLO jet cross sections was too slow to be used iteratively in the fit. Thus, they were used to compute LO and NLO weights, $\tilde{\sigma}$, which are independent of α_s and the PDFs, and are obtained by integrating the corresponding partonic hard cross sections[3] in bins of

[3] For the dijet photoproduction cross sections, the weights also included the convolution with the photon PDFs.

ξ (the proton momentum fraction carried by the incoming parton), μ_F (the factorisation scale) and, for the case $\mu_F \neq \mu_R$, μ_R (the renormalisation scale). The NLO QCD cross sections, for each measured bin, were then obtained by folding these weights with the PDFs and α_s according to the formula

$$\sigma = \sum_n \sum_a \sum_{i,j,k} f_a(\langle\xi\rangle_i, \langle\mu_F\rangle_j) \cdot \alpha_s^n(\langle\mu_R\rangle_k) \cdot \tilde{\sigma}^{(n)}_{a,\{i,j,k\}} \;, \quad (2)$$

where the three sums run over the order n in α_s, the flavour a of the incoming parton, and the indices (i, j, k) of the ξ, μ_F and μ_R bins, respectively. The PDF, f_a, and α_s were evaluated at the mean values $\langle\xi\rangle$, $\langle\mu_F\rangle$ and $\langle\mu_R\rangle$ of the variables ξ, μ_F and μ_R in each (i, j, k) bin. The factorisation scale was chosen as $\mu_F = Q$ for the DIS jets, and the renormalisation scale was chosen as $\mu_R = E_T^B$ (with $\mu_R = Q$ as a cross-check). For the photoproduced dijets, the standard scale choices were $\mu_R = \mu_F = E_T/2$ (where E_T is the summed transverse momenta of final-state partons). This procedure reproduces the NLO predictions to better than 0.5%.

The predictions were multiplied by hadronisation corrections before they were used to fit the data. These were determined by using Monte Carlo (MC) programmes, which model parton hadronisation to estimate the ratio of the hadron- to parton-level cross sections for each bin. For the DIS jet data, an average of the values obtained using the Ariadne, Lepto and Herwig MC programmes was taken [13]. For the photoproduction data, an average of the values obtained from the Herwig and Pythia MC programmes was taken [14]. The hadronisation corrections are generally within a few percent of unity [13, 14]. The predictions for DIS jet production were also corrected for Z^0 contributions.

3.3 Parameterisation of PDFs

The PDFs for u valence, d valence, total sea, gluon and the difference between the d and u contributions to the sea, are each parameterised, at $Q_0^2 = 7$ GeV^2, by the form

$$xf(x) = p_1 x^{p_2}(1-x)^{p_3}(1+p_4 x).$$

It was checked that no significant improvement in χ^2 results from the use of more complex polynomial forms or from variation of the value of Q_0^2. The following constraints were imposed on the parameters p_i:

- the normalisation parameters p_1, for the d and u valence and for the gluon, were constrained by imposing the number sum-rules and momentum sum-rule, respectively;
- the p_2 parameters, which constrain the low-x behaviour of the valence distributions, were set equal for u and d, since there is insufficient information to constrain any difference;

- there is also no information on the flavour structure of the light-quark sea in a fit to ZEUS data alone. Thus, the normalisation of the $\bar{d} - \bar{u}$ distribution was fixed to be consistent with the measured violation of the Gottfried sum-rule [33, 34] and its shape was fixed to be consistent with the Drell-Yan data [35];
- a suppression of the strange sea by a factor of two at Q_0^2 was imposed in accordance with neutrino induced dimuon data from CCFR-NuTeV [36, 37].

The fit is not sensitive to reasonable variations of these assumptions, indicating that it is only possible to extract a flavour-averaged sea distribution from these ZEUS data.

The ZEUS inclusive cross-section data are statistics limited at large x, where the sea and the gluon distributions are small. This leads to sizeable uncertainties in the mid- to high-x sea and gluon shapes if a fit is made to inclusive cross-section data alone. The ZEUS jet data constrain the gluon distribution in this kinematic region. Two different strategies were used to constrain the sea distribution: firstly, a simple parameterisation setting $p_4 = 0$ was used; secondly, the p_4 parameter was freed but the p_3 parameter was fixed to the value obtained in the ZEUS-S global fit [8]. In the latter case, model uncertainties on the high-x sea include the effect of changing this fixed value of p_3 within the limits of its uncertainty as determined in the global fit. There is very little difference in the shapes and uncertainties of the sea PDF as determined in these two strategies once this model uncertainty on p_3 is taken into account. Distributions are presented for the former choice because of its simplicity. Finally, there are 11 free parameters describing the input PDF distributions, which are listed in Table 2.

4 Results

The ZEUS-JETS fit and the NC and CC reduced cross-section data are shown in Figs. 1, 2 and 3. The fit and the jet cross-section data are illustrated in Figs. 4 and 5. A good description of the data is obtained over many orders of magnitude in scale. A measure of the goodness of fit for the Offset method is obtained by re-evaluating the χ^2 by adding the statistical, uncorrelated and correlated systematic uncertainties in quadrature [24]. The total χ^2 obtained is 470 for 577 data points. The extracted PDF parameters and their experimental uncertainties are given in Table 2.

The valence distributions for the ZEUS-JETS fit are shown in Fig. 6. Although the high-x valence distributions are not as well constrained as they are in global fits which include fixed-target data, they are competitive, particularly for the less well-known d valence distribution. Furthermore, they are free from uncertainties due to heavy-target corrections, higher-twist effects and isospin-symmetry assumptions.

The gluon and sea distributions for the ZEUS-JETS fit are shown together in Fig. 7. Whereas the sea distribution rises at low x for all Q^2, the gluon distribution flattens for $Q^2 \sim 2.5$ GeV^2 and becomes valence-like for lower Q^2. The gluon and sea distributions are as well determined as the corresponding distributions of the global fits [1–3, 8] at low x since the HERA inclusive NC data determine these distributions for all the fits. At high x, the uncertainties of the sea are constrained to be similar to those of the ZEUS-S global fit by the choice of parameterisation, whereas the uncertainties of the gluon have been reduced by the addition of the ZEUS jet data.

In Fig. 8 the uncertainty of the gluon distribution for fits with and without the jet data are compared. The shapes of the PDFs are not changed significantly by the addition of jet data, even though the gluon parameterisation is sufficiently flexible to allow this, indicating that there is no tension between the jet data and the inclusive cross-section data. Although the jet data constrain the gluon mainly in the range $0.01 \lesssim \xi \lesssim 0.4$, the momentum sum-rule ensures that the indirect constraint of these data is still significant at higher x. The decrease in the uncertainty on the gluon distribution is striking; for example at $Q^2 = 7$ GeV^2 and $x = 0.06$ the uncertainty is reduced from 17% to 10%. A similar decrease in uncertainty by a factor of about two is found in this mid-x range, over the full Q^2 range.

In Fig. 9, the valence, sea and gluon PDFs are compared for the ZEUS-JETS fit and the previous ZEUS-S global PDF analysis. There is good agreement between the ZEUS PDF extractions. The figure also compares the MRST and CTEQ PDFs to the ZEUS-JETS PDFs. These PDFs are compatible with the ZEUS PDFs, considering the size of the uncertainties on each of the PDF sets.

4.1 PDF Uncertainties

The following sources of model uncertainty have been included in the PDF uncertainty bands:

- the value of Q_0^2 was varied in the range $4 < Q_0^2 < 10$ GeV^2;
- the forms of the input PDF parameterisations were changed, by modifiying the form $(1 + p_4 x)$ to $(1 + p_4 x + p_5\sqrt{x})$ for the valence parameterisations and by varying the choice of constraints applied to the sea parameterisation as explained in Section 3;
- the standard E_T cuts applied to the jet data were raised to $E_T^B > 10$ GeV and $E_T^{\rm jet1} > 17$ GeV for DIS jets and photoproduced jets, respectively, since there are some small discrepancies between the fit predictions and the jet data at the lowest

transverse energies[4];

- the hadronisation corrections applied to the jet data have been varied by half the difference between the values obtained from the HERWIG and PYTHIA MC programmes for the photoproduced jet cross sections [14] and by the variance of the values obtained from the ARIADNE, LEPTO and HERWIG MC programmes for the DIS jet cross sections [13]. The uncertainties on the hadronisation corrections determined by these procedures are $< 1\%$; they lead to uncertainties in the PDFs which are small in comparison to the experimental uncertainties;
- as explained in Section 3.2, the photoproduction data used in the fit are enriched with direct photon processes by the cut $x_\gamma^{\rm obs} > 0.75$; however it is not possible to select jet cross sections that are completely independent of photon structure. Therefore the sensitivity of the fit results to the input photon PDFs was investigated. In Fig. 10a the proton PDFs extracted from the ZEUS-JETS fit using the AFG photon PDFs [28] are compared with those extracted using the GRV [38,39] and CJK [40] photon PDFs. There is no visible difference in the extracted proton PDFs. In Fig. 10b this comparison is shown for a fit in which the 'resolved' photon cross sections, $x_\gamma^{\rm obs} < 0.75$ [14], have been included. A significant difference is now observed between the extracted proton PDFs using the AFG, GRV, or CJK photon PDFs. Note that this difference is greatest in the region of x where the jet data have the most significant impact in reducing the uncertainty of the gluon PDF. Thus, although the addition of the resolved photoproduction cross sections reduces the experimental uncertainty on the extracted gluon PDF, it introduces a model uncertainty due to the limited knowledge of the photon PDFs which outweighs this advantage. Hence the present analysis used only the photoproduction cross sections with $x_\gamma^{\rm obs} > 0.75$. The difference in the proton PDFs extracted using the AFG and GRV photon PDFs was used to estimate the small residual model uncertainty due to the photon PDF in the ZEUS-JETS fit.

The effect of some of the larger model variations listed above on the shapes of the extracted PDFs is illustrated in Fig. 11. These model variations are a much smaller source of uncertainty than the experimental uncertainties.

In addition to these model uncertainties a variety of cross-checks have been made:

- the minimum x of data entering the fit was raised to $x > 5 \times 10^{-4}$, and the minimum Q^2 of data entering the fit was raised to $Q^2 > 4.5$ GeV^2. These variations did not produce any significant changes in the PDF parameters;
- the ZMVFN heavy quark production scheme wasused instead of the TRVFN scheme. The jet data are all at sufficiently high scale that the TRVFN and ZMVFN schemes

[4] This is also the case for the MRST and CTEQ PDFs [13,14].

are equivalent. However, it is well known that the use of the ZMVFN scheme makes small differences to the shape of the gluon at $x < 10^{-3}$. This shift is well within the experimental uncertainty bands;

- the choices of factorisation and renormalisation scale have been varied. The choice of Q is not in dispute for inclusive DIS processes. However, the scale choices for jet-production are not so unambiguous. Thus, factorisation and renormalisation scales were varied by a factor of $\sqrt{2}$ for both the DIS jets and the photoproduced jets and additionally the conventional scale $\mu_F = \mu_R = Q$ for the inclusive cross-section data was varied by the same factor[5]. The renormalisation scale for the DIS jet data was also changed from $\mu_R = E_T^B$ to $\mu_R = Q$. These changes in the choice of scale produced changes in the shapes of the PDFs which are small in comparison to the experimental uncertainties;

- a Hessian fit was performed to the same data sets as for the ZEUS-JETS fit. The central values of the PDF parameters were found to be similar to those of the ZEUS-JETS fit, well within the latter's uncertainties. In the Hessian fitting method [25,26], the theoretical prediction is used to determine the optimal correlated systematic shifts of the data. The correlated systematic uncertainties are assumed to be Gaussian distributed. This assumption is not correct for the data sets considered here, and the resulting uncertainties of the fit are underestimated. On the other hand, the method has a χ^2 which is a well defined measure of the goodness-of-fit, not available in the Offset method. The χ^2 per degree of freedom of the Hessian fit was 1.12 for 566 degrees of freedom[6].

Figure 12 shows the ZEUS-JETS PDFs compared to those of the H1 2000 PDF analysis [10]. The comparison is done in terms of the $xU = x(u + c)$, $x\bar{U} = x(\bar{u} + \bar{c})$, $xD = x(d + s)$, $x\bar{D} = x(\bar{d} + \bar{s})$ and gluon PDFs, which have been directly extracted by H1. The PDFs extracted by ZEUS and H1 are broadly compatible. Note that the Hessian method of treatment of the correlated systematic uncertainties used in the H1 fit results in a smaller experimental uncertainty on the gluon PDF [25], but the model uncertainty is significant. By contrast, the Offset method of treatment of correlated systematic uncertainties used in the ZEUS fit results in a larger experimental uncertainty, so that it dominates in comparison to the model uncertainties.

---

[5] Larger variations, by a factor of 2, are not presented since they produce fits with unacceptably large χ^2. The acceptability of a χ^2 is judged by the hypothesis testing criterion [8] such that the variation from the minimum should not exceed $\sim \sqrt{2N}$, where N is the number of degrees of freedom. In the ZEUS-JETS fit, $\sqrt{2N} = 33$.

[6] If the E_T cuts applied to the jet data are raised, as described in Section 4.1, the χ^2 per degree of freedom of the Hessian fit becomes 1.01 for 554 degrees of freedom.

4.2 Comparison to Tevatron jet data

It has been suggested that PDF fits to DIS data alone cannot produce a hard enough high-x gluon to describe the high-E_T inclusive jet cross sections measured at the Tevatron [1]. To investigate this issue, the ZEUS-JETS PDFs were used to make predictions for the CDF jet cross sections. The information on the correlated systematic uncertainties of the CDF data is supplied in such a way that it is possible to make a fit to these data by the Hessian method. In such a fit, the PDF parameters are fixed but the eight systematic uncertainties are freed. The χ^2 of the CDF jet data with respect to the ZEUS-JETS fit was calculated using this procedure and $\chi^2 = 48.9$ was obtained. This is to be compared to $\chi^2 = 46.8$ which was obtained by the CDF collaboration [12], using the same procedure, for a fit to the CTEQ4HJ PDFs, which were specially developed to fit the CDF jet data. Thus, the ZEUS-JETS PDFs give an acceptable description of the CDF jet data.

5 Extraction of α_s

The strong correlation between the gluon shape and the value of $\alpha_s(M_Z)$, which affects fits to inclusive cross-section data alone, can be broken by including the jet production cross-section data, which are dependent on the gluon PDF and the value $\alpha_s(M_Z)$ in a different way from the total cross section. Jet production cross sections are directly dependent on the gluon PDF through the BGF process, but jet production also proceeds though the QCDC process, which dominates the cross section at large scales. This process depends on $\alpha_s(M_Z)$ and the quark densities, which are directly determined from the inclusive cross-section data. Thus the addition of jet data allows an extraction of $\alpha_s(M_Z)$ that is not strongly correlated to the shape of the gluon PDF.

In previous determinations of $\alpha_s(M_Z)$ using ZEUS jet data [13, 41–45], the uncertainty from the correlation to the PDFs was taken into account by using PDFs from the global fits of CTEQ and MRST, which were determined assuming different values of $\alpha_s(M_Z)$. In the present analysis this correlation is directly included by fitting the PDF parameters and $\alpha_s(M_Z)$ simultaneously. The conditions for the ZEUS-JETS-α_s fit are otherwise the same as for the ZEUS-JETS fit. The value

$$\alpha_s(M_Z) = 0.1183 \pm 0.0007(\text{uncorr.}) \pm 0.0022(\text{corr.}) \pm 0.0016(\text{norm.}) \pm 0.0008(\text{model})$$

was obtained, where the four uncertainties arise from the following sources: statistical and other uncorrelated sources; experimental correlated systematic sources excluding normalisation uncertainties; normalisation uncertainties; and model uncertainty. Here the uncertainty on $\alpha_s(M_Z)$, which usually comes from the correlation to the PDF shapes, is automatically included in the experimental uncertainties. The sources of model uncertainty were discussed in Section 4.1. In addition to the model uncertainties included in the PDF extraction, the following extra sources have been included in the model uncertainty for $\alpha_s(M_Z)$: variation of the Q^2 and x cuts on the data, as specified in Section 4.1; and the use of the ZMVFN instead of the RTVFN scheme for heavy quark production.

This extraction is at NLO. A crude estimate of the effect of terms beyond NLO can be made by variation of the choice of μ_R. This scale was varied by a factor of $\sqrt{2}$ for all the data sets entering into the fit, as described in Section 4.1. The most significant effect comes from the variation of the renormalisation scale for the photoproduction process. These scale changes produced shifts of $\Delta\alpha_s(M_Z) \sim \pm 0.005$.

Figure 13 illustrates that the improved accuracy of the extraction of $\alpha_s(M_Z)$ in the ZEUS-JETS-α_s fit is due to the inclusion of the jet data. The χ^2 profile around the minimum is shown as a function of $\alpha_s(M_Z)$ for the ZEUS-JETS-α_s fit and a similar fit in which the jet data are not included. The value of $\alpha_s(M_Z)$ extracted is in agreement with recent determinations using measurements in DIS [8, 9, 13, 41–44, 46] and photoproduction of jets [45] at HERA and with the current world average of 0.1182 ± 0.0027 [47, 48].

The extracted value of $\alpha_s(M_Z)$ is close to the fixed value used in the ZEUS-JETS fit, and there are therefore no significant changes in the central values of the PDF parameters. The uncertainties of the valence and sea PDFs are also unaffected. However, there is some increase in the overall uncertainty of the gluon PDF because a weak correlation remains between $\alpha_s(M_Z)$ and the gluon PDF parameters. This is illustrated for various Q^2 values in Fig. 14.

The input of the jet data results in a much reduced uncertainty on the extracted value of $\alpha_s(M_Z)$ compared to the previous ZEUS-α_s analysis [8]. Since the present analysis was performed within a single experiment, the contributions from normalisation uncertainties and from correlated systematic uncertainties are both significantly reduced. In consequence, the total uncertainty on the gluon, including the uncertainty due to $\alpha_s(M_Z)$, is reduced in comparison to the total gluon uncertainty determined in the ZEUS-α_s global fit.

6 Summary

Due to the precision and kinematic coverage of the ZEUS data, it is now possible to extract proton PDFs and $\alpha_s(M_Z)$ in a fit to data from a single experiment with minimal external input. The ZEUS high-Q^2 cross sections were used to constrain the valence PDFs, ZEUS low-Q^2 NC data were used to constrain the low-x sea and gluon distributions and ZEUS data on jet production were used to constrain the mid- to high-x gluon. This provides a compelling demonstration of QCD factorisation, showing that NLO QCD in the framework of the Standard Model is able to simultaneously describe inclusive cross sections and jet cross sections. The additional constraint on the gluon PDF from the jet production data allows an accurate extraction of the value of $\alpha_s(M_Z)$ in NLO QCD,

$$\alpha_s(M_Z) = 0.1183 \pm 0.0028(\text{exp.}) \pm 0.0008(\text{model}).$$

The uncertainty in $\alpha_s(M_Z)$ due to terms beyond NLO has been estimated as $\Delta\alpha_s(M_Z) \sim \pm 0.005$, by variation of the choice of scales. This is the first extraction of $\alpha_s(M_Z)$ from HERA data alone.

The total uncertainty on the gluon PDF is reduced in comparison to the ZEUS-α_s global fit because of the greater precision of the $\alpha_s(M_Z)$ measurement. The uncertainties on the valence PDFs are becoming competitive with those of the global fits, and they are not subject to uncertainties from heavy-target corrections, higher-twist contributions or isospin-symmetry assumptions. The precision of PDFs extracted from the global fits is now limited by the systematic uncertainties of the contributing experiments, whereas the precision of the present fit using ZEUS data only is limited by the statistical uncertainties and so further improvement can be expected when higher precision HERA-II data become available.

Acknowledgements

We thank the DESY directorate for their strong support and encouragememt. The remarkable achievements of the HERA machine group were essential for the successful completion of this work and are greatly appreciated. The design, construction and installation of the ZEUS detector has been made possible by the effort of many people who are not listed as authors. We acknowledge helpful discussions with Robert Thorne and Dick Roberts.

References

[1] A.D. Martin et al., Eur. Phys. J. **C 23**, 73 (2002).

[2] A.D. Martin et al., Eur. Phys. J. **C 28**, 455 (2002).

[3] J. Pumplin et al., JHEP **0207**, 012 (2002).

[4] V.N. Gribov and L.N. Lipatov, Sov. J. Nucl. Phys. **15**, 438 (1972).

[5] L.N. Lipatov, Sov. J. Nucl. Phys. **20**, 94 (1975).

[6] G. Altarelli and G. Parisi, Nucl. Phys. **B 126**, 298 (1977).

[7] Yu.L. Dokshitzer, Sov. Phys. JETP **46**, 641 (1977).

[8] ZEUS Collab., S. Chekanov et al., Phys. Rev. **D 67**, 012007 (2003).

[9] H1 Collab., C. Adloff et al., Eur. Phys. J. **C 21**, 33 (2001).

[10] H1 Collab., C. Adloff et al., Eur. Phys. J. **C 30**, 1 (2003).

[11] DØ Collab., B. Abbott et al., Phys. Rev. Lett. **82**, 2451 (1999).

[12] CDF Collab., T.Affolder et al., Phys. Rev. **D 64**, 032001 (2001).

[13] ZEUS Collab., S. Chekanov et al., Phys. Lett. **B 547**, 164 (2002).

[14] ZEUS Collab., S. Chekanov et al., Eur. Phys. J. **C 23**, 615 (2002).

[15] ZEUS Collab., S. Chekanov et al., Eur. Phys. J. **C 21**, 443 (2001).

[16] ZEUS Collab., J. Breitweg et al., Eur. Phys. J. **C 12**, 411 (2000).

[17] ZEUS Collab., S. Chekanov et al., Eur. Phys. J. **C 28**, 175 (2003).

[18] ZEUS Collab., S. Chekanov et al., Phys. Lett. **B 539**, 197 (2002).

[19] ZEUS Collab., S. Chekanov et al., Phys. Rev. **D 70**, 052001 (2004).

[20] ZEUS Collab., S. Chekanov et al., Eur. Phys. J. **C 32**, 16 (2003).

[21] Particle Data Group, S. Eidelman et al., Phys. Lett. **B 592**, 1 (2004).

[22] G. Altarelli and G. Martinelli, Phys. Lett. **B 76**, 89 (1978).

[23] M. Botje, *QCDNUM version 16.12* (unpublished), available on `http://www.nikhef.nl/~h24/qcdcode/index.html`.

[24] M. Botje, J. Phys. **G 28**, 779 (2002).

[25] A.M. Cooper-Sarkar, J. Phys. **G 28**, 2609 (2002).

[26] R.S. Thorne et al., J. Phys. **G 28**, 2717 (2002).

[27] R.G. Roberts and R.S. Thorne, Phys. Rev. **D 57**, 6871 (1998).

[28] P. Aurenche, J.P. Guillet and M. Fontannaz, Z. Phys. **C 64**, 621 (1994).

[29] ZEUS Collab., M. Derrick et al., Phys. Lett. **B 348**, 665 (1995).

[30] ZEUS Collab., M. Derrick et al., Phys. Lett. **B 322**, 287 (1994).

[31] S. Frixione and G. Ridolfi, Nucl. Phys. **B 507**, 315 (1997).

[32] S. Catani and M.H. Seymour, Nucl. Phys. **B 510**, 503 (1998).

[33] P. Amaudruz et al., Phys. Lett. **B 295**, 159 (1992).

[34] P. Amaudruz et al., Phys. Rev. Lett. **66**, 2712 (1991).

[35] R.S. Towell et al., Phys. Rev. **D 64**, 052002 (2002).

[36] CCFR Collab., A.O. Bazarko et al., Z. Phys. **C 65**, 189 (1995).

[37] G. P. Zeller et al., Phys. Rev. Lett. **88**, 091802 (2002).

[38] M. Glück, E. Reya and A. Vogt, Phys. Rev. **D 45**, 3986 (1992).

[39] M. Glück, E. Reya and A. Vogt, Phys. Rev. **D 46**, 1973 (1992).

[40] C. Cornet, P. Jankowski and M. Krawczyk, Phys. Rev. **D 70**, 093004 (2004).

[41] ZEUS Collab., J. Breitweg et al., Phys. Lett. **B 507**, 70 (2001).

[42] ZEUS Collab., S. Chekanov et al., Eur. Phys. J. **C 31**, 149 (2003).

[43] ZEUS Collab., S. Chekanov et al., Phys. Lett. **B 558**, 41 (2003).

[44] ZEUS Collab., S. Chekanov et al., Nucl. Phys. **B 700**, 3 (2004).

[45] ZEUS Collab., S. Chekanov et al., Phys. Lett. **B 560**, 7 (2003).

[46] H1 Collab., C. Adloff et al., Eur. Phys. J. **C 19**, 289 (2001).

[47] S. Bethke, J. Phys. **G 26**, R27 (2000).

[48] S. Bethke, Preprint hep-ex/0407021, 2004.

Data Set	Ndata	Norm	Nsys	Kinematic range of the data
NC e^+p 96-97 [15]	242	2% (1%)	10 1,2,3,4,5,6,7,8,9,10	$2.7 < Q^2 < 30,000$ GeV^2 $6.3 \times 10^{-5} < x < 0.65$
CC e^+p 94-97 [16]	29	2%	3 5,6,11	$280 < Q^2 < 17,000$ GeV^2 $0.015 < x < 0.42$
NC e^-p 98-99 [17]	92	1.8%	6 12,13,14,15,16,11	$200 < Q^2 < 30,000$ GeV^2 $0.005 < x < 0.65$
CC e^-p 98-99 [18]	26	1.8%	3 17,18,11	$280 < Q^2 < 17,000$ GeV^2 $0.015 < x < 0.42$
NC e^+p 99-00 [19]	90	2%	8 12,13,14,15,19,11,20,21	$200 < Q^2 < 30,000$ GeV^2 $0.005 < x < 0.65$
CC e^+p 99-00 [20]	30	2%	3 17,-18,11	$280 < Q^2 < 17,000$ GeV^2 $0.008 < x < 0.42$
DIS jets e^+p 96-97 [13]	30	2%	1 22	$125 < Q^2 < 30,000$ GeV^2 $8 < E_T^B < 100$ GeV
γp dijets 96-97 [14] $x_\gamma^{\rm obs} > 0.75$	38	2%	1 22	$14 < E_T^{\rm jet1} < 75$ GeV

Table 1: *The number of data points (Ndata), normalisation uncertainties (Norm) and number of point-to-point correlated systematic uncertainties (Nsys) are detailed for each of the data sets used in the ZEUS-JETS fit. The kinematic regions of the data sets are also given. The number of independent correlated systematic uncertainties is specified as follows. Each independent source of uncertainty is assigned a number in the order of the systematic uncertainties as given in the corresponding publication. These numbers are given in the column headed Nsys, for each data set. For example, for the CC e^+p 94-97 data set, the first two systematic uncertainties are fully correlated to the fifth and sixth systematic uncertainties for the NC e^+p 96-97 data set. Note also that the second systematic uncertainty for the CC e^+p 99-00 data set is fully anti-correlated to the second systematic uncertainty for the CC e^-p 98-99 data. The normalisation uncertainties are applied as follows. There are two normalisation uncertainties for the NC e^+p 96-97 data: an overall uncertainty and the relative uncertainty (indicated in parentheses) of the data with $Q^2 < 30 GeV^2$, with respect to the higher Q^2 data. The CC e^+p 94-97 data are dominated by the 96-97 data, so that the same overall normalisation uncertainty is applied to this data set. The two jet production data sets also share the overall normalisation uncertainty of the 96/97 data. The NC and CC e^-p 98-99 data share a common normalisation uncertainty as do the NC and CC e^+p 99-00 data.*

PDF	p_1	p_2	p_3	p_4
xu_v	$(3.1 \pm 0.7 \pm 1.2)$	$0.64 \pm 0.05 \pm 0.08$	$4.06 \pm 0.18 \pm 0.24$	$2.3 \pm 1.1 \pm 1.0$
xd_v	$(1.7 \pm 0.3 \pm 0.5$	$0.63 \pm 0.05 \pm 0.08$	$4.8 \pm 0.7 \pm 1.0$	$2.6 \pm 2.2 \pm 2.3$
xS	$0.72 \pm 0.03 \pm 0.10$	$-0.217 \pm 0.005 \pm 0.020$	$7.0 \pm 0.8 \pm 2.0$	0
xg	$(0.9 \pm 0.1 \pm 0.3)$	$-0.28 \pm 0.02 \pm 0.04$	$10.2 \pm 0.7 \pm 2.1$	$16 \pm 4 \pm 10$

Table 2: *Table of PDF parameters at $Q_0^2 = 7$ GeV^2, as determined from the ZEUS-JETS fit. The first uncertainty given originates from statistical and other uncorrelated sources and the second uncertainty is the additional contribution from correlated systematic uncertainties. The numbers in parentheses were derived from the fitted parameters via the number and momentum sum-rules.*

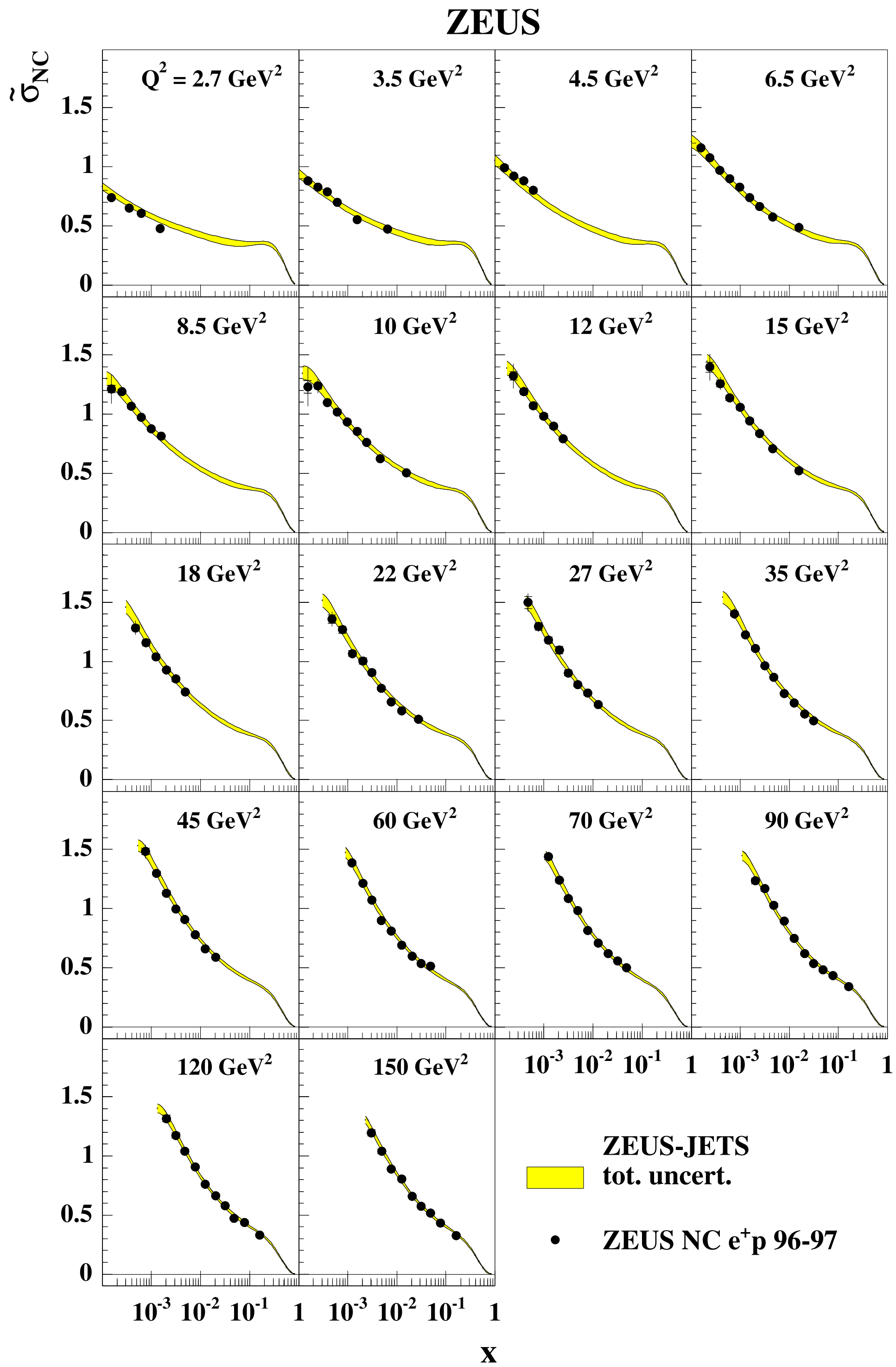

Figure 1: *ZEUS-JETS fit compared to ZEUS low-Q^2 e^+p NC reduced cross sections, $\tilde{\sigma}_{\mathrm{NC}}$.*

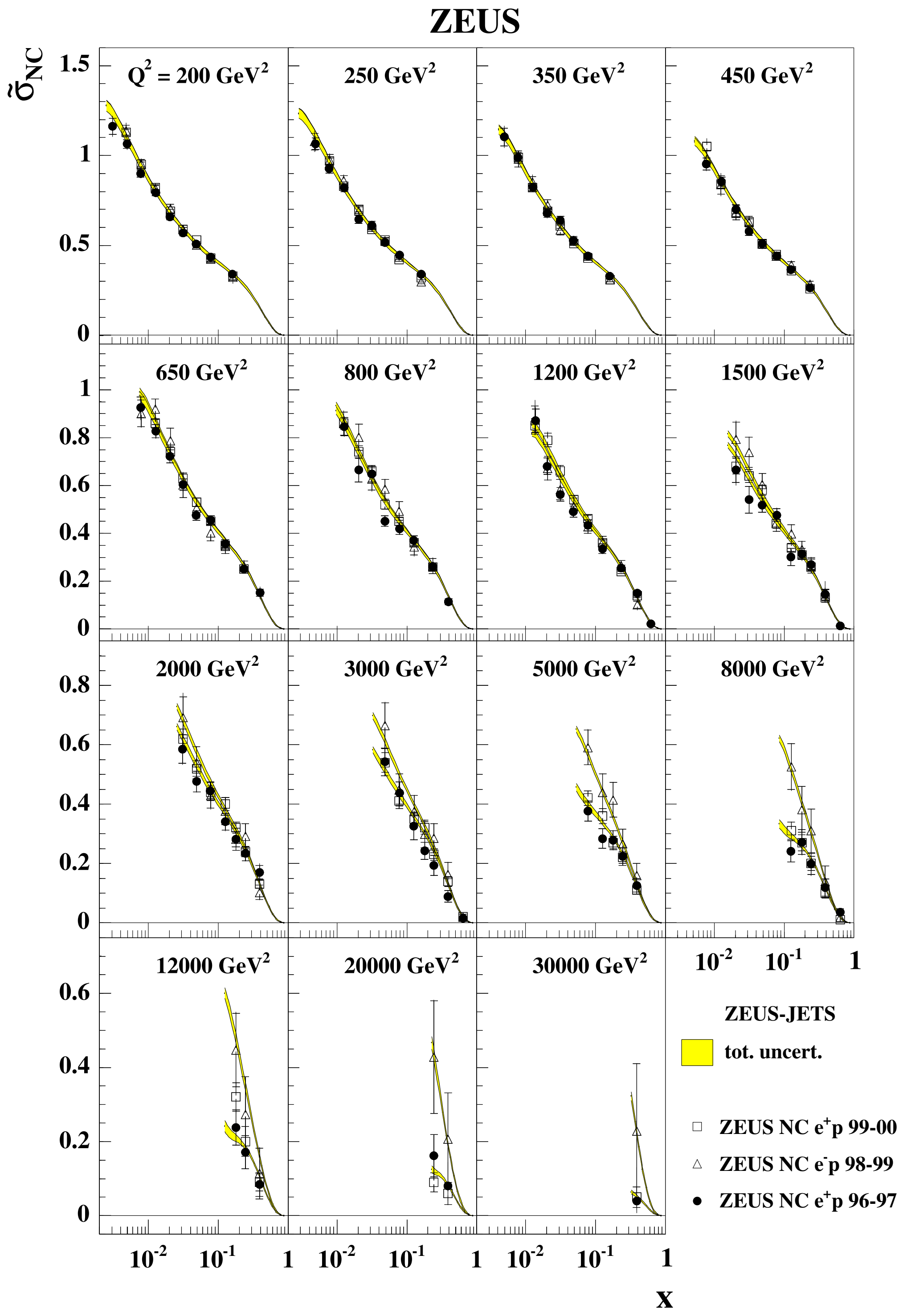

Figure 2: *ZEUS-JETS fit compared to ZEUS high-Q^2 NC e^+p and e^-p reduced cross sections, $\tilde{\sigma}_{\mathrm{NC}}$.*

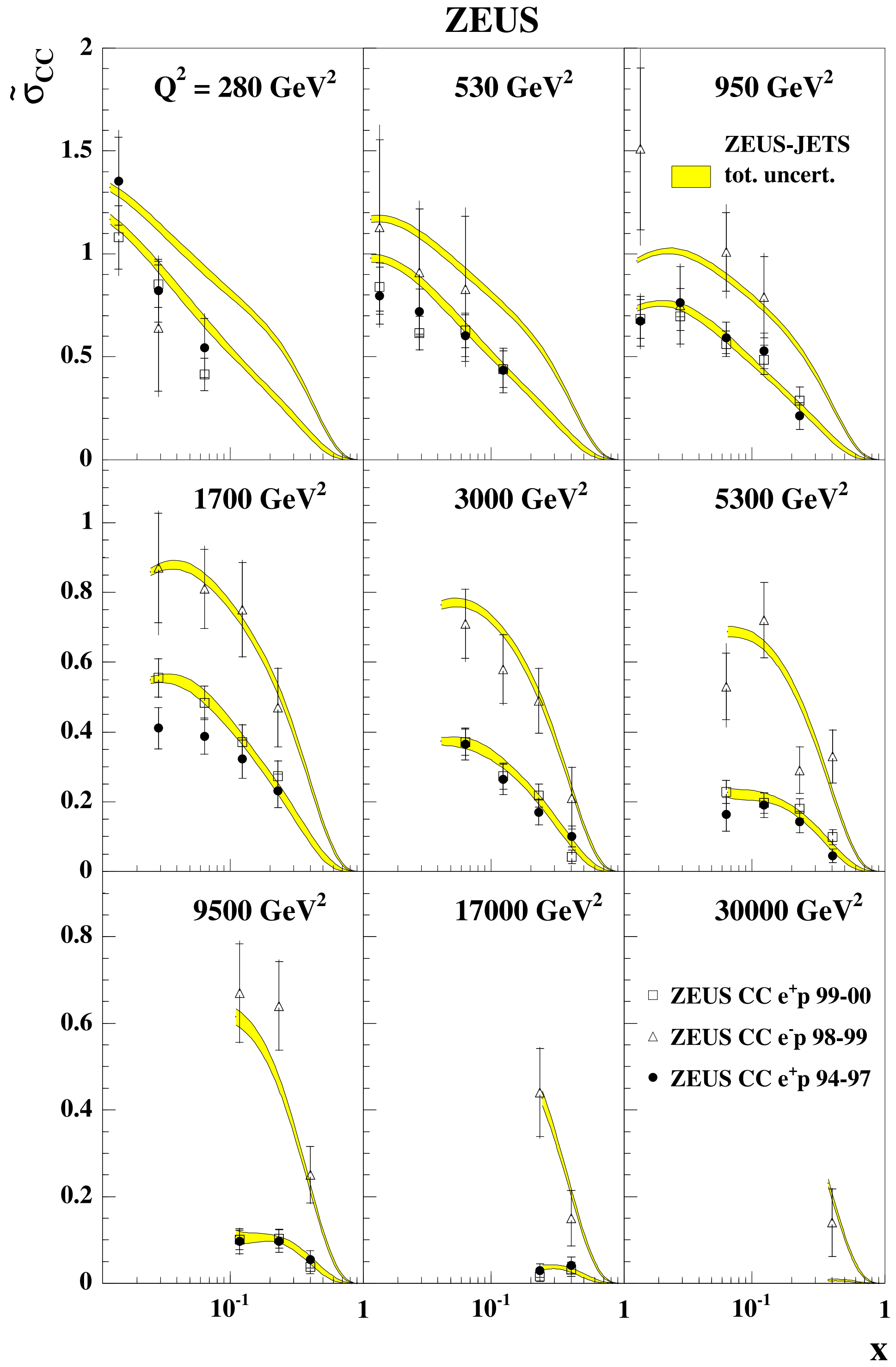

Figure 3: *ZEUS-JETS fit compared to ZEUS high-Q^2 CC e^+p and e^-p reduced cross sections, $\tilde{\sigma}_{\rm CC}$.*

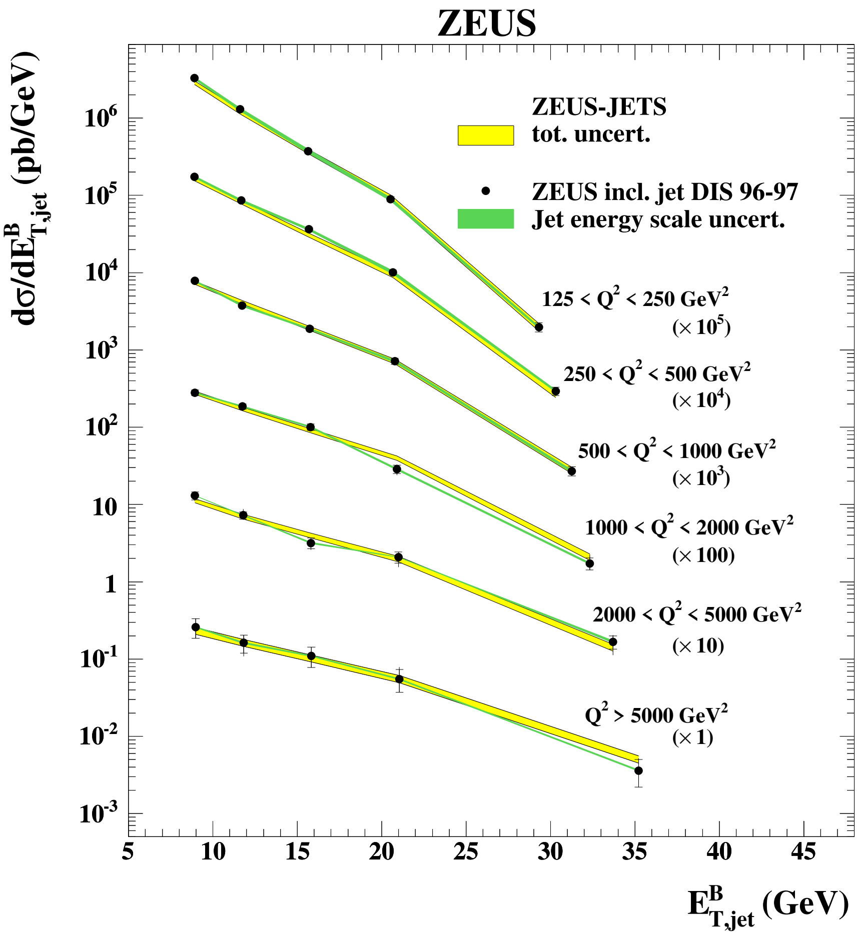

Figure 4: *ZEUS-JETS fit compared to ZEUS DIS jet data. Each cross section has been multiplied by the scale factor in brackets to aid visibility.*

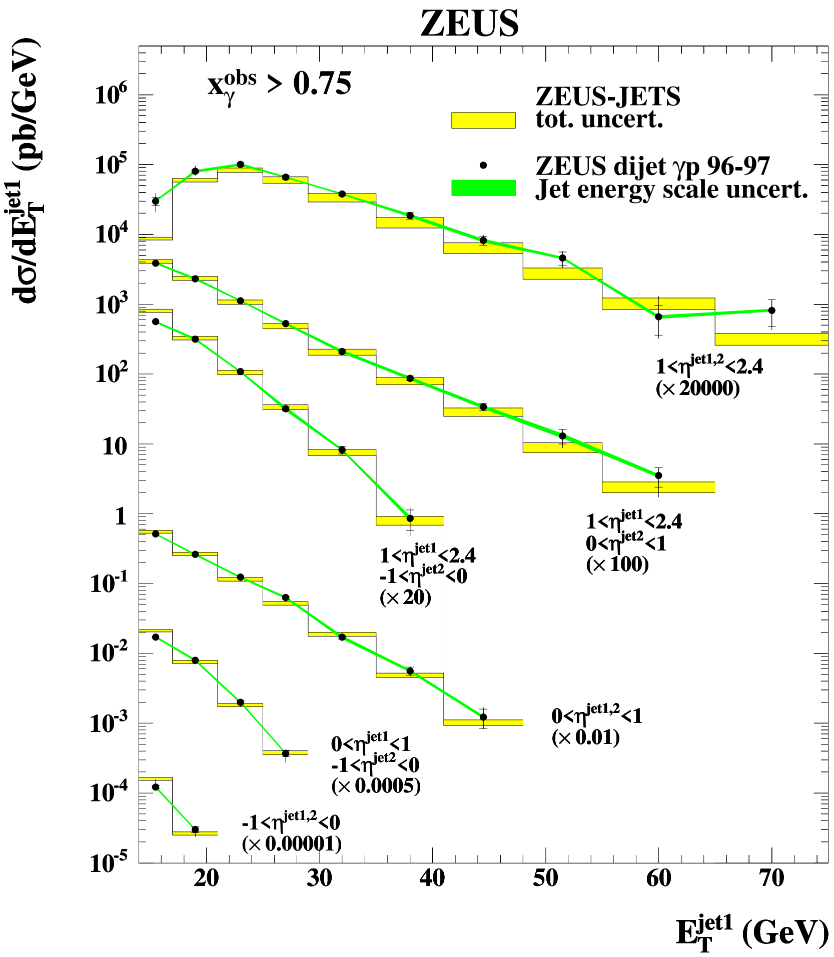

Figure 5: *ZEUS-JETS fit compared to photoproduced dijet data. Each cross section has been multiplied by the scale factor in brackets to aid visibility.*

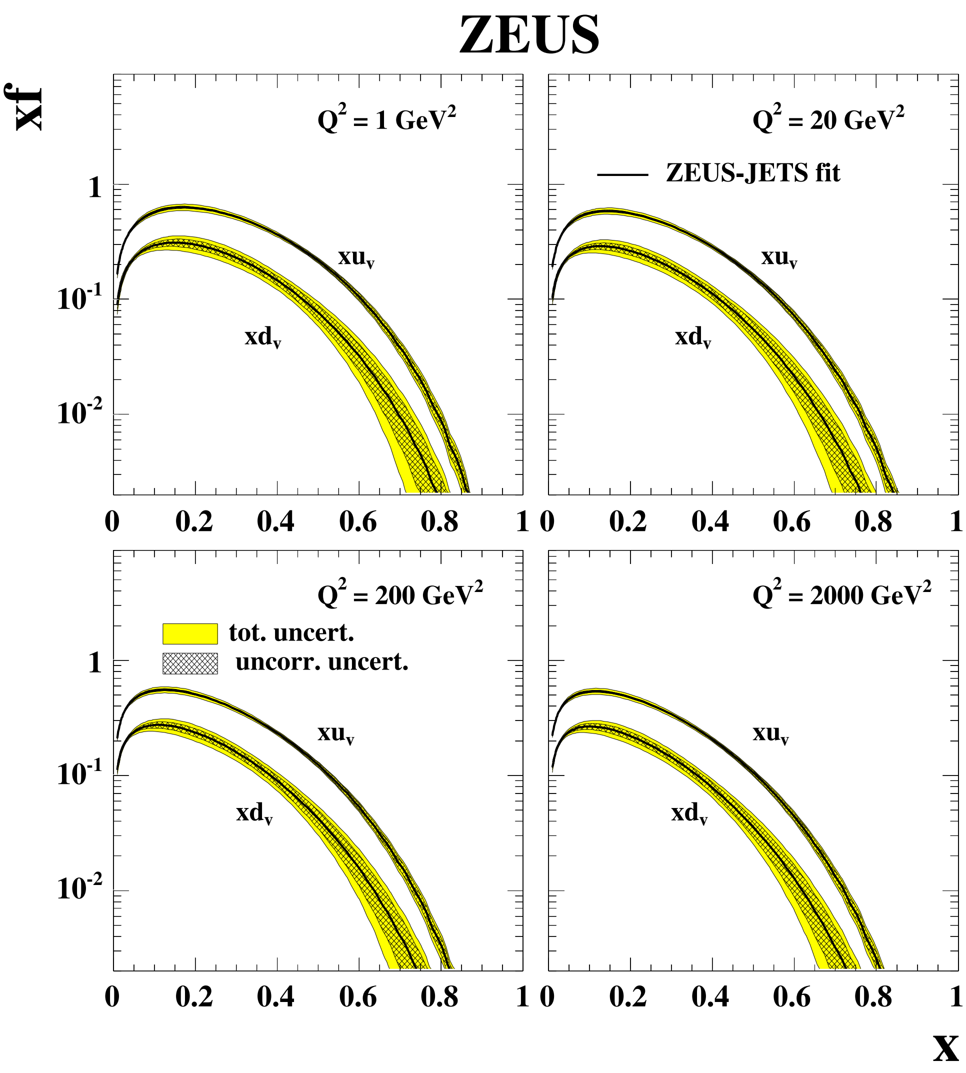

Figure 6: *Valence PDFs extracted from the ZEUS-JETS fit. The inner cross-hatched error bands show the statistical and uncorrelated systematic uncertainty, the grey error bands show the total uncertainty including experimental correlated systematic uncertainties, normalisations and model uncertainty.*

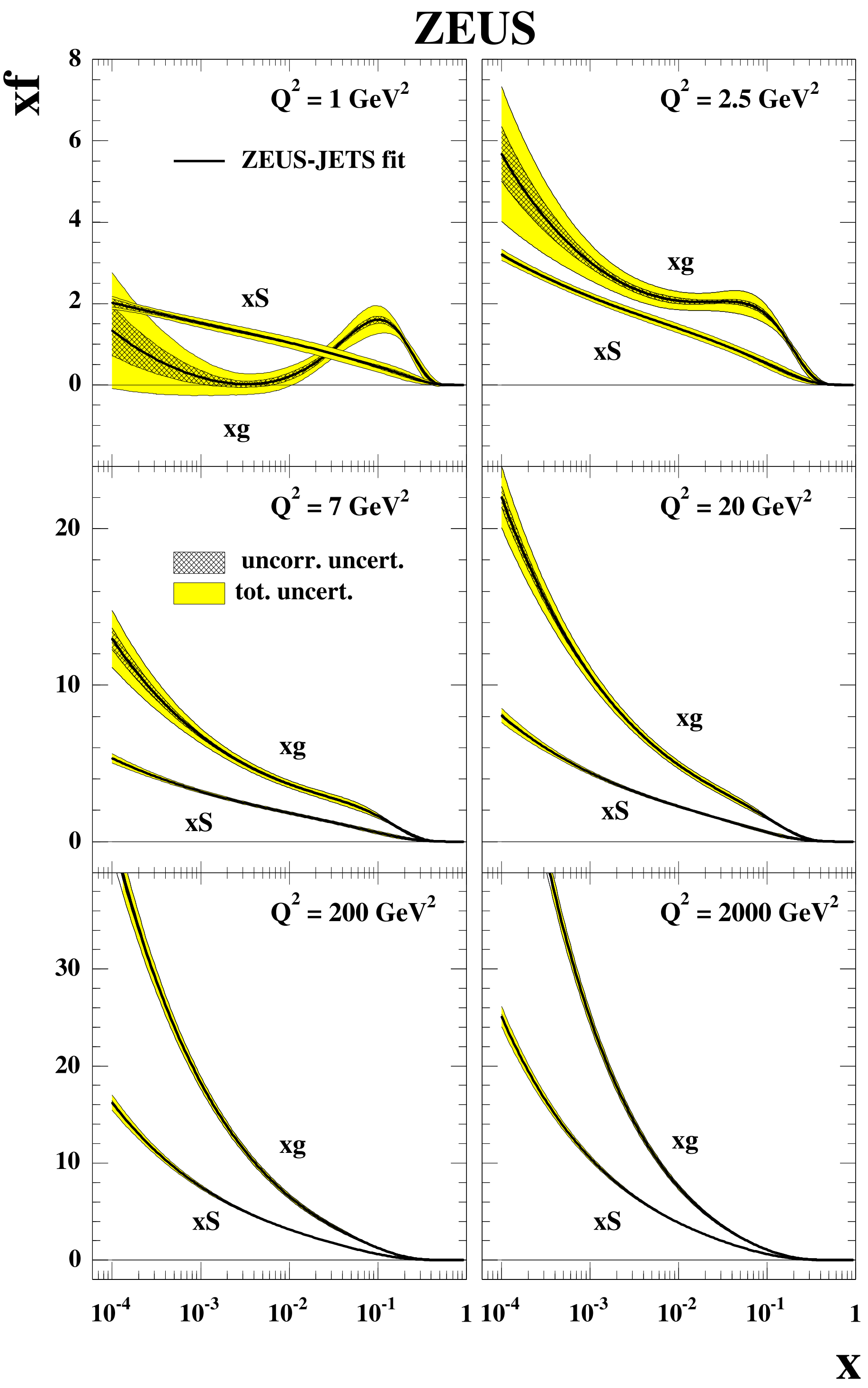

Figure 7: *Gluon and sea PDFs extracted from the ZEUS-JETS fit. The uncorrelated and total error bands are as in the caption to Fig. 6.*

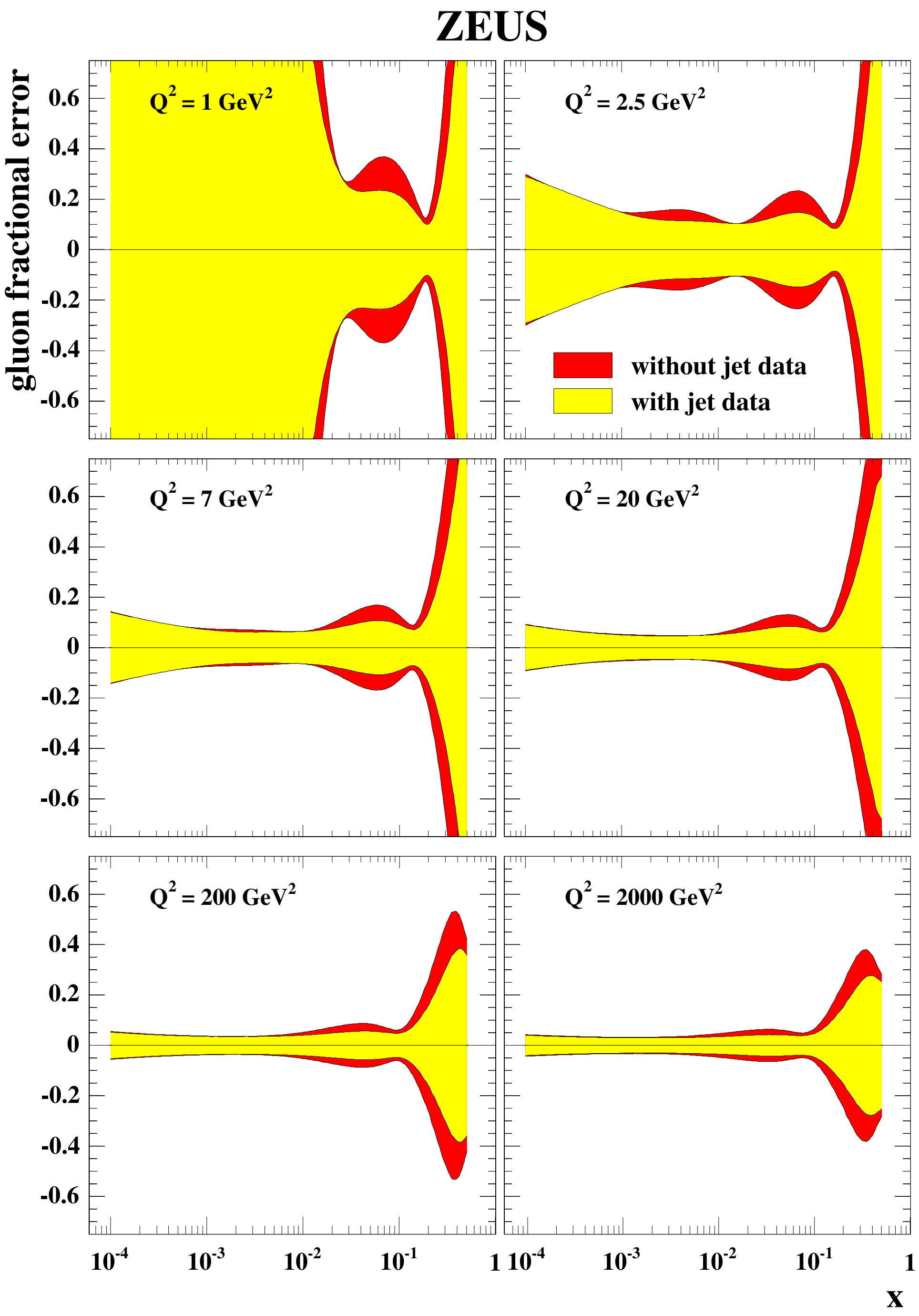

Figure 8: *The total experimental uncertainty on the gluon PDF for the ZEUS-JETS fit (central error bands) compared to the total experimental uncertainty on the gluon PDF for a fit not incuding the jet data (outer error bands). The uncertainties are shown as fractional differences from the central values of the fits, for various values of Q^2. The total experimental uncertainty includes the statistical, uncorrelated and correlated systematic uncertainties and normalisations, for both fits.*

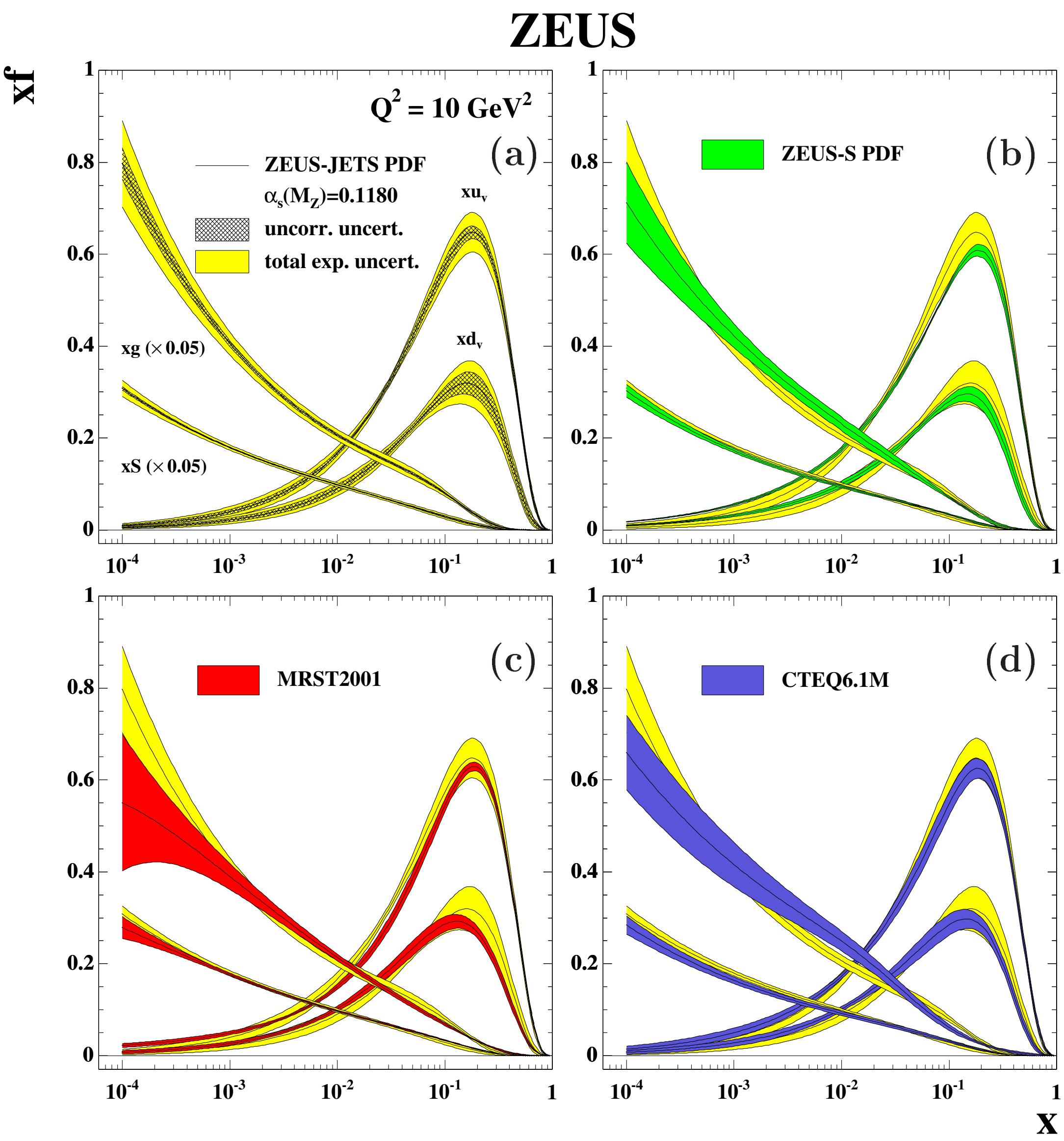

Figure 9: *(a) PDFs extracted from the ZEUS-JETS fit. (b) PDFs extracted from the ZEUS-JETS fit compared to ZEUS-S PDFs. (c) PDFs extracted from the ZEUS-JETS fit compared to MRST2001 PDFs. (d) PDFs extracted from the ZEUS-JETS fit compared to CTEQ6.1 PDFs. The total experimental uncertainty bands are shown for each PDF set.*

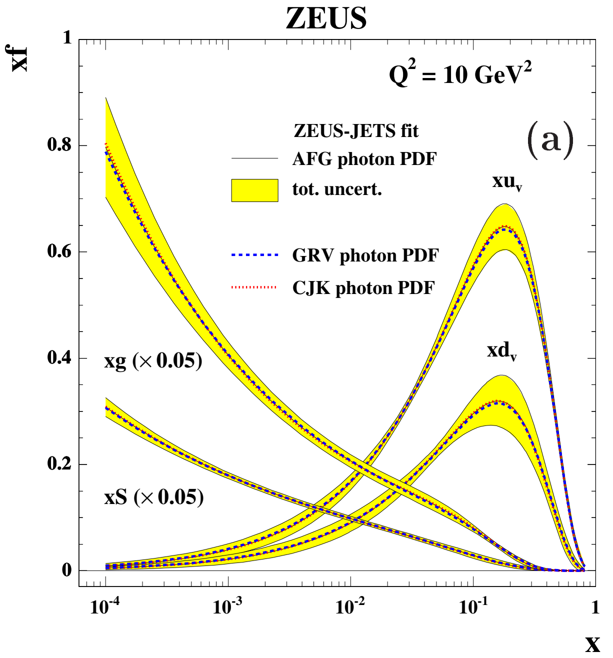

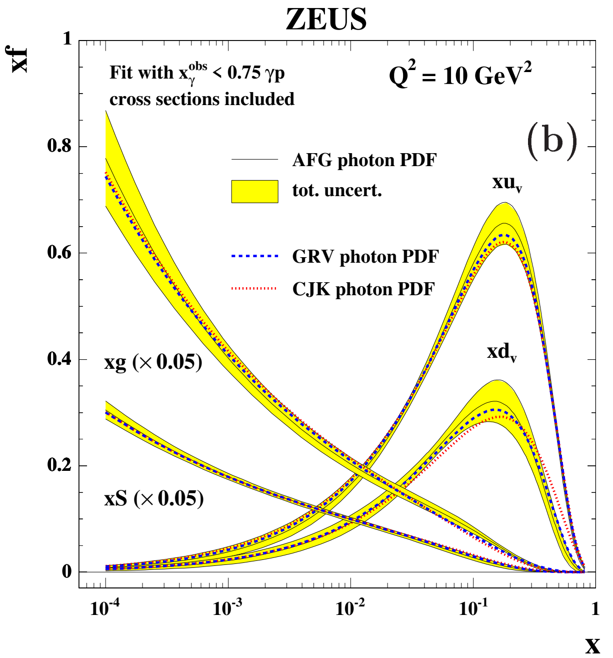

Figure 10: *(a) PDFs extracted from the ZEUS-JETS fit using different photon PDFs. The AFG photon PDF is used to obtain the central line, the GRV photon PDF gives the dashed line and the CJK photon PDF gives the dotted line. (b) PDFs extracted from a fit in which the resolved photoproduction cross-sections are included in addition to all the standard data sets for the ZEUS-JETS fit. The AFG photon PDF is used to obtain the central line, the GRV photon PDF gives the dashed line and the CJK photon PDF gives the dotted line. The total experimental error bands shown in these figures were obtained using the AFG photon PDF; for details see the caption to Fig. 8.*

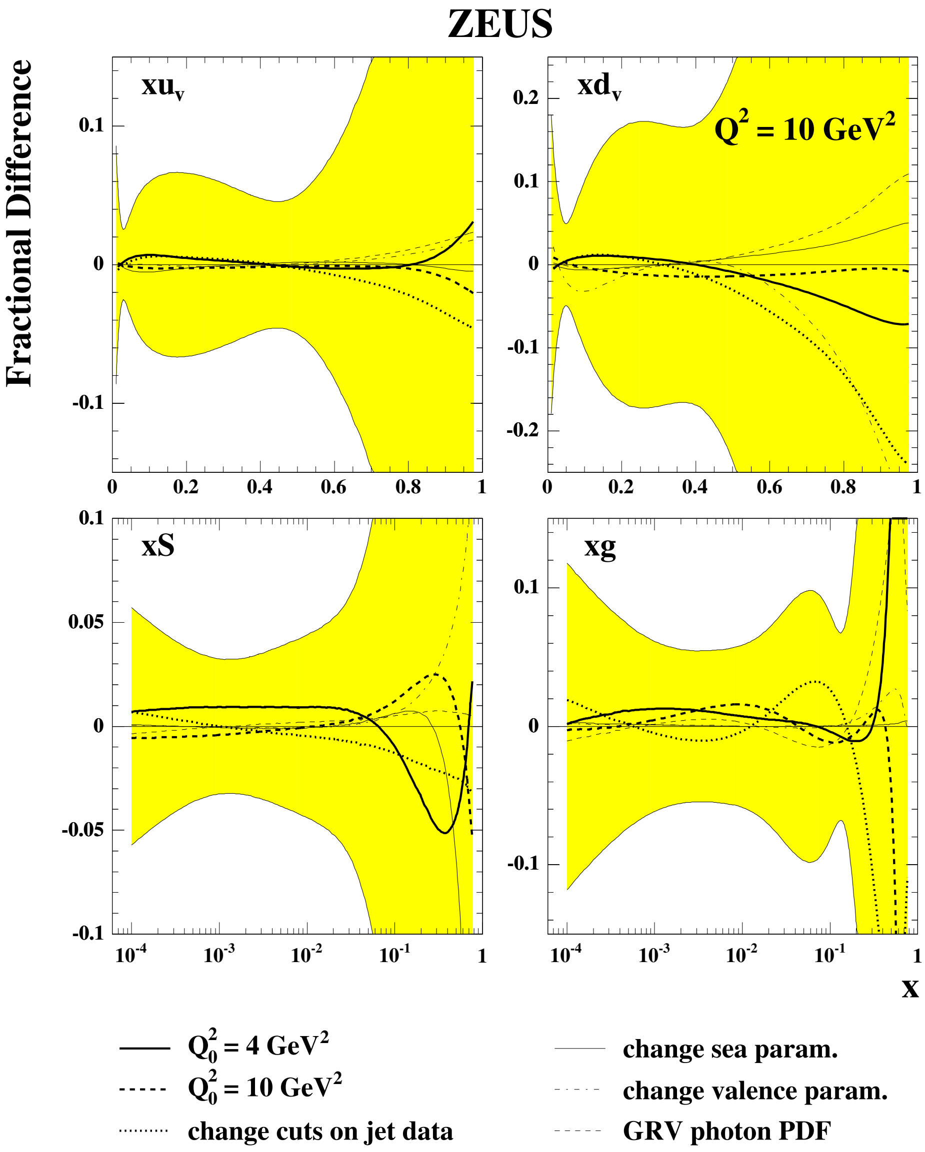

Figure 11: *Model variations discussed in the text are illustrated as fractional differences from the ZEUS-JETS central value for all the PDFs. For comparison, the shaded band shows the total experimental uncertainty.*

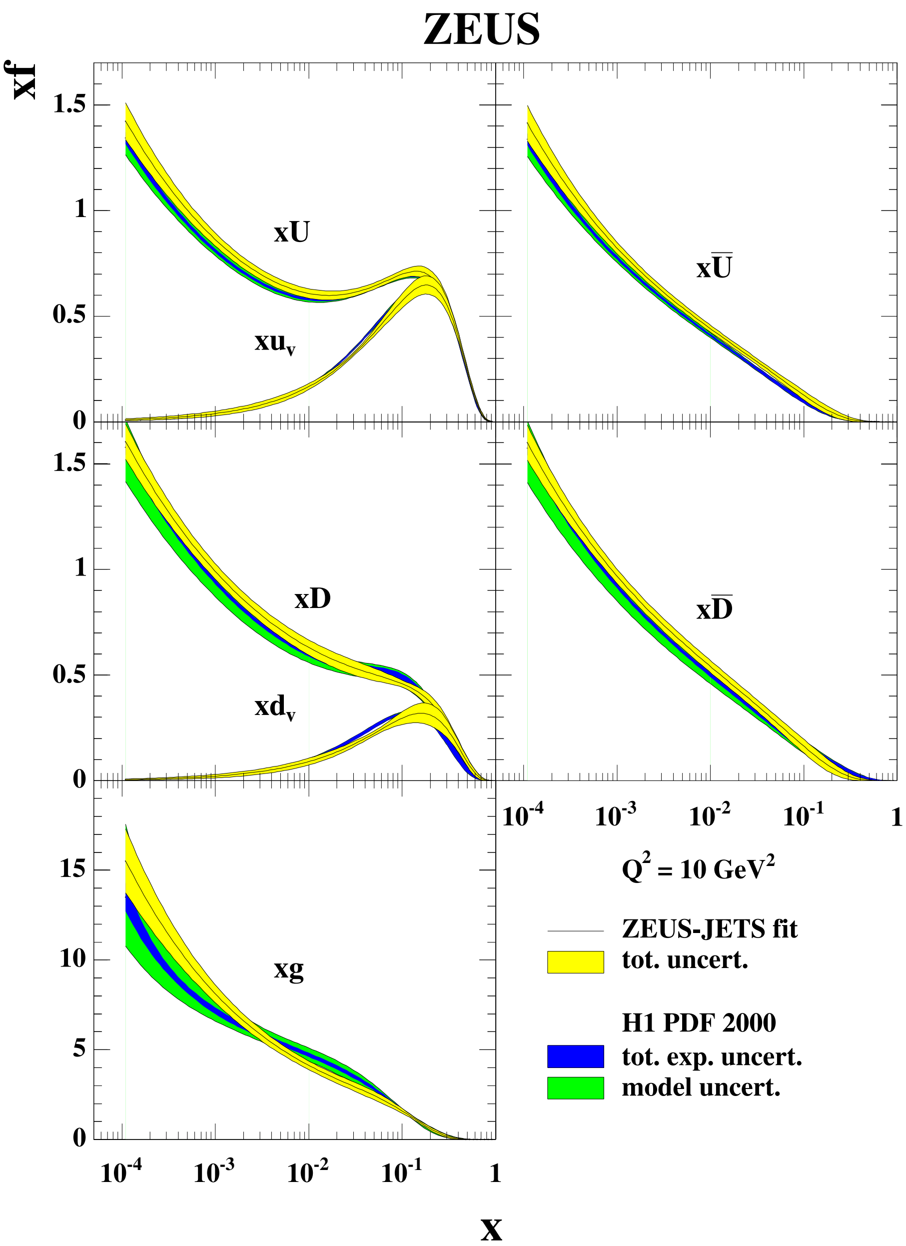

Figure 12: *Comparison of the PDFs extracted from the ZEUS-JETS fit with those extracted in the H1 2000 PDF analysis. For each analysis the total experimental error bands and the model error bands are included. However, the model uncertainty is not visible for the ZEUS-JETS fit.*

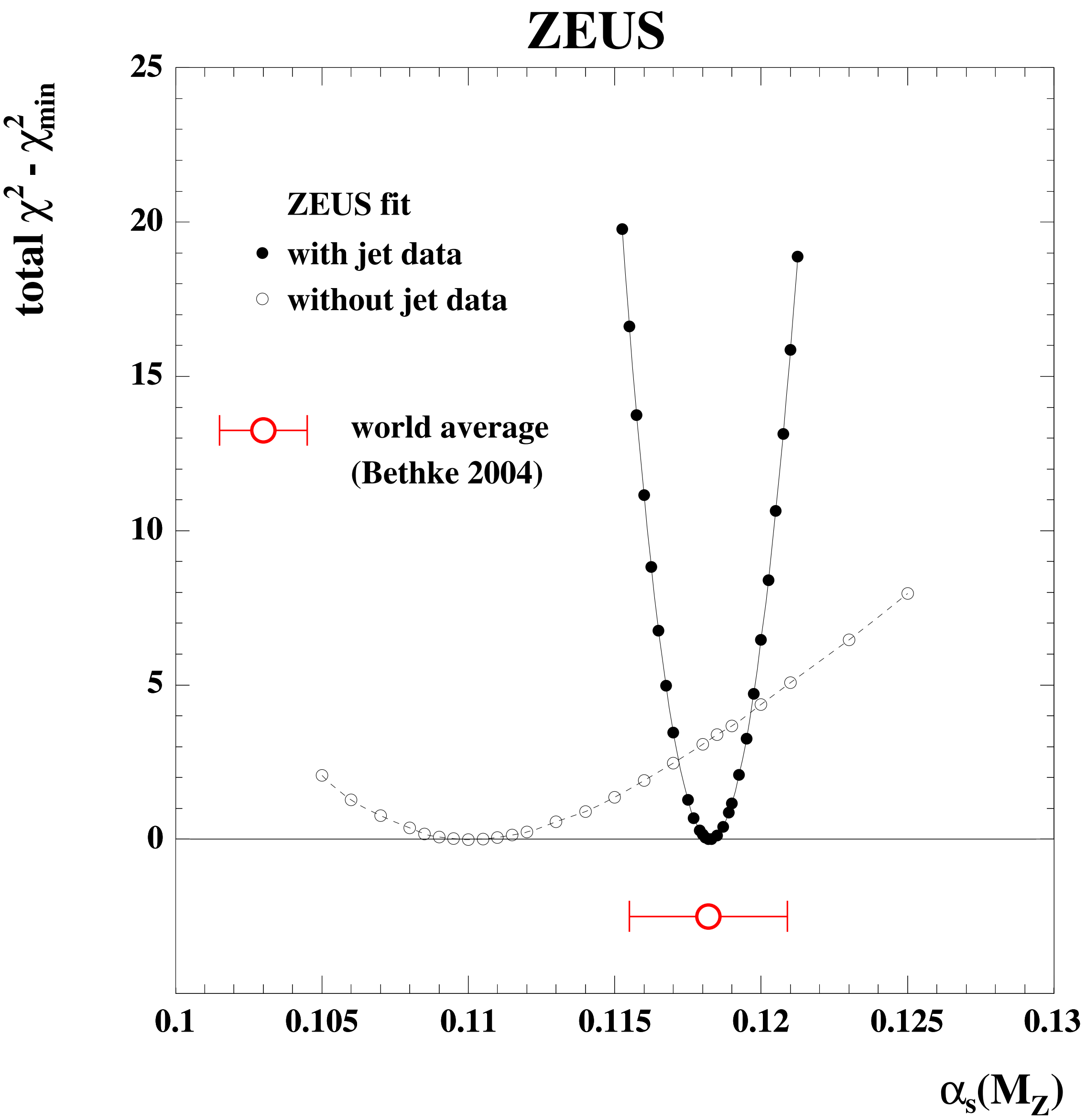

Figure 13: *The χ^2 profile as a function of $\alpha_s(M_Z)$ for the ZEUS-JETS-α_s fit (black dots) and for a similar fit not including the jet data (clear dots). The ordinate is given in terms of the difference between the total χ^2 and the minimum χ^2, for each fit.*

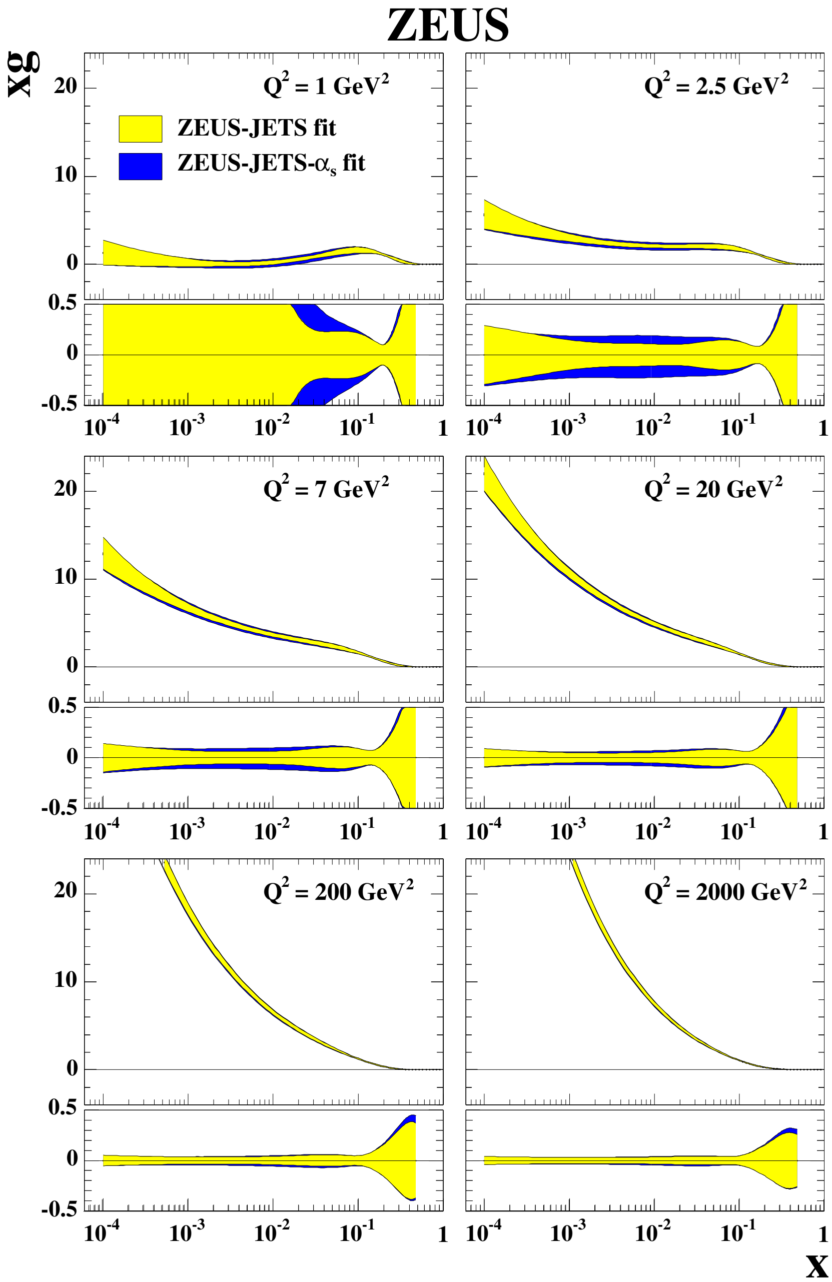

Figure 14: *Gluon distributions extracted from the ZEUS-JETS-α_s fit. The uncertainties on these distributions are shown beneath each distribution as fractional differences from the central value. The inner error bands show the total uncertainty including statistical, uncorrelated and correlated experimental systematic uncertainties, normalisations and model uncertainties and the outer error bands show the additional uncertainty in the gluon coming from the variation of $\alpha_s(M_Z)$.*